HAC E7324

CR-180819

8-CM ION THRUSTER CHARACTERIZATION

F.J. Wessel, D.J. Hancock, C.R. Dulgeroff, and W.S. Williamson

Hughes Research Laboratories
3011 Malibu Canyon Road
Malibu, CA 90265

October 1987

NAS 3-22447
Supplementary Final Report

March 1982 through February 1983

(NASA-CR-180819) AN 8-cm ION THRUSTER CHARACTERIZATION Supplementary Final Report, Mar. 1982 - Feb. 1983 (Hughes Research Labs.) 57 p Avail: NTIS HC A04/MF A01 CSCL 21H G3/20

N88-10106

Unclas
0102764

NATIONAL AERONAUTICS AND SPACE ADMINISTRATION
Lewis Research Center
Cleveland, OH 44135

NASA
National Aeronautics and Space Administration

Report Documentation Page

1. Report No.	2. Government Accession No.	3. Recipient's Catalog No.
NASA CR-180819		

4. Title and Subtitle	5. Report Date
8-cm Ion Thruster Characterization: Supplementary Final Report	October 1987
	6. Performing Organization Code

7. Author(s)	8. Performing Organization Report No.
F.J. Wessel, D.J. Hancock, C.R. Dulgeroff, and W.S. Williamson	
	10. Work Unit No.

9. Performing Organization Name and Address	11. Contract or Grant No.
Hughes Research Laboratories 3011 Malibu Canyon Road Malibu, CA 90265	NAS 3-22447
	13. Type of Report and Period Covered
12. Sponsoring Agency Name and Address	Supplementary Final Report 3/82 - 2/83
National Aeronautics and Space Administration Lewis Research Center Cleveland, OH 44135	14. Sponsoring Agency Code

15. Supplementary Notes

NASA Program Manager: Maris Mantenieks

16. Abstract

The performance of the Ion Auxiliary Propulsion System (IAPS) thruster was increased to thrust T = 32 mN, specific impulse I_{sp} = 4062 s, and thrust-to-power ratio T/P = 33 mN/kW. This performance was obtained by increasing the discharge power, accelerating voltage, propellant flow rate, and chamber magnetic field. Adding a plenum and main vaporizer for propellant distribution was the only major change required in the thruster. The modified thruster characterization is presented. A cathode-magnet assembly did not improve performance. A simplified power processing unit was designed and evaluated. This unit decreased the parts count of the IAPS power processing unit by a factor of ten.

17. Key Words (Suggested by Author(s))	18. Distribution Statement
Ion propulsion Mercury ion thruster Discharge chamber IAPS Simplified power processing	Unclassified, Unlimited

19. Security Classif. (of this report)	20. Security Classif. (of this page)	21. No. of pages	22. Price
Unclassified	Unclassified	62	

PREPARATION OF THE REPORT DOCUMENTATION PAGE

The last page of a report facing the third cover is the Report Documentation Page, RDP. Information presented on this page is used in announcing and cataloging reports as well as preparing the cover and title page. Thus it is important that the information be correct. Instructions for filling in each block of the form are as follows:

Block 1. Report No. NASA report series number, if preassigned.

Block 2. Government Accession No. Leave blank.

Block 3. Recipient's Catalog No. Reserved for use by each report recipient.

Block 4. Title and Subtitle. Typed in caps and lower case with dash or period separating subtitle from title.

Block 5. Report Date. Approximate month and year the report will be published.

Block 6. Performing Organization Code. Leave blank.

Block 7. Author(s). Provide full names exactly as they are to appear on the title page. If applicable, the word editor should follow a name.

Block 8. Performing Organization Report No. NASA installation report control number and, if desired, the non-NASA performing organization report control number.

Block 9. Performing Organization Name and Address. Provide affiliation (NASA program office, NASA installation, or contractor name) of authors.

Block 10. Work Unit No. Provide Research and Technology Objectives and Plans (RTOP) number.

Block 11. Contract or Grant No. Provide when applicable.

Block 12. Sponsoring Agency Name and Address. National Aeronautics and Space Administration, Washington, D.C. 20546-0001. If contractor report, add NASA installation or HQ program office.

Block 13. Type of Report and Period Covered. NASA formal report series; for Contractor Report also list type (interim, final) and period covered when applicable.

Block 14. Sponsoring Agency Code. Leave blank.

Block 15. Supplementary Notes. Information not included elsewhere: affiliation of authors if additional space is required for block 9, notice of work sponsored by another agency, monitor of contract, information about supplements (film, data tapes, etc.), meeting site and date for presented papers, journal to which an article has been submitted, note of a report made from a thesis, appendix by author other than shown in block 7.

Block 16. Abstract. The abstract should be informative rather than descriptive and should state the objectives of the investigation, the methods employed (e.g., simulation, experiment, or remote sensing), the results obtained, and the conclusions reached.

Block 17. Key Words. Identifying words or phrases to be used in cataloging the report.

Block 18. Distribution Statement. Indicate whether report is available to public or not. If not to be controlled, use "Unclassified-Unlimited." If controlled availability is required, list the category approved on the Document Availability Authorization Form (see NHB 2200.2, Form FF427). Also specify subject category (see "Table of Contents" in a current issue of STAR), in which report is to be distributed.

Block 19. Security Classification (of this report). Self-explanatory.

Block 20. Security Classification (of this page). Self-explanatory.

Block 21. No. of Pages. Count front matter pages beginning with iii, text pages including internal blank pages, and the RDP, but not the title page or the back of the title page.

Block 22. Price Code. If block 18 shows "Unclassified-Unlimited," provide the NTIS price code (see "NTIS Price Schedules" in a current issue of STAR) and at the bottom of the form add either "For sale by the National Technical Information Service, Springfield, VA 22161-2171" or "For sale by the Superintendent of Documents, U.S. Government Printing Office, Washington, DC 20402-0001," whichever is appropriate.

FOREWORD

The Extended-Performance 8-cm Ion Thruster and associated Simplified Power Processor Unit described in this Supplementary Final Report were assembled and evaluated by personnel of Hughes Research Laboratories (HRL), Malibu, California. The work was done in the Plasma Physics Department, managed by Dr. J. Hyman, Jr. The Lewis Research Center supported the work under NASA Contract NAS 3-22447, 8-CM Ion Thruster Characterization. M.E. Mantenieks was the NASA Program Manager. The HRL Program Manager, F.J. Wessel, shared the responsibility of assembling and evaluating the Simplified Power Processor Unit with D.J. Hancock. Other HRL personnel contributing to the program were R.L. Poeschel, J.R. Beattie, W.S. Williamson, C.R. Dulgeroff, R.R. Robson, M.W. Sawins, A.R. Kramer, D.R. Deane, and R.L. Maheux.

TABLE OF CONTENTS

LIST OF ILLUSTRATIONS

LIST OF ILLUSTRATIONS (CONTINUED)

LIST OF TABLES

SECTION 1

INTRODUCTION

This report documents work conducted at Hughes Research Laboratories from March 1982 through February 1983, under NASA Lewis Research Center Contract No. NAS 3-22447. These activities build on earlier work conducted under the same contract, which is reported in an earlier final report (NASA document No. CR-167887).[1] The present work consisted of two tasks: (1) extending the 8-cm thruster performance obtained earlier[1] and (2) simplifying the power processor control unit for the 8-cm thruster. By describing these tasks, this supplementary Final Report completes the program's documentation.

In the original effort (August 1980 to October 1981), the performance of the Ion Auxiliary Propulsion System (IAPS) thruster was improved by altering the thruster operating parameters and component hardware. The baseline values (i.e., before contract modification) of the IAPS thruster[2] included:

- Thrust, T =5 mN
- Specific impulse, I_{sp} = 2900 s
- Ion beam current, I_B = 72 mA
- Thrust-to-power ratio, T/P = 36 mN/kW.

By the end of the original effort with a modified thruster, we had achieved the following improvements (the actual thrust-to-power ratio is not quoted because the nonoptimal thermal design of the laboratory thruster produces an unrealistically favorable comparison):

- T = 25 mN
- I_{sp} = 4300 s
- I_B = 310 mA.

The first task under the present effort improved those performance values to T = 32 mN, I_{sp} = 4062 s, I_B = 338 mA, and T/P = 33 mN/kW (for these measurements, a realistic value of the thrust-to-power ratio was available from the data*). Having attained these values, we then simplified the thruster power electronics in the second task. For operating the thruster, new power conditioning and thruster-control concepts were developed and implemented in a simplified power-processing unit (SPPU). The new design substantially reduced the parts count and the complexity of the original power processor. To verify these concepts, a laboratory-model simplified power-processor unit (SPPU) was built to operate an IAPS-type thruster. After activation of a single switch, the SPPU provided complete autonomous thruster startup and control.

Results from testing the thruster and SPPU are presented in Sections 2 and 3.

---

* These performance data include a correction corresponding to additional vaporizer power that would be required in a flight thruster. In our laboratory model, the vaporizers were coupled too closely to the hot discharge chamber, resulting in unrealistically low vaporizer power levels.

SECTION 2

THRUSTER TESTS

Thruster modifications described in this section achieved a thrust level of T = 32 mN with a specific impulse of I_{SP} = 4062 s, and a thrust-to-power level of T/P = 33 mN/kW. After obtaining baseline data with the thruster shell biased alternatively at cathode potential and at keeper potential, we investigated the following:

- Propellant diversion with different baffles
- Performance with shortened chamber
- Performance of nominal chamber with added plenum and vaporizer
- Performance with cathode magnets.

The test results of these configurations follow.

A. CATHODE- OR KEEPER-POTENTIAL-BIASED SHELL

These activities began with the thruster modified in the manner described below. Its design features include a standard IAPS divergent magnetic-field pattern, the discharge-chamber magnetic-field strength increased to 15 mT (IAPS value: 11 mT, measured at the downstream end of the cathode polepiece), a propellant-diversion baffle of 2.38-cm diameter (IAPS value: 2.06-cm diameter), small-hole accel grid (SHAG) optics, and heat-sunk vaporizers. In addition, a simple flat washer (of suitable dimension) that greatly improved access to the cathode-isolator-vaporizer assembly replaced the standard IAPS thruster rear shield. This design change permitted direct electrical connections between the vacuum bulkhead and the thruster components, and shortened each thruster disassembly/assembly cycle.

In the first test configuration, a MACOR washer electrically isolated the discharge-chamber shell from the cathode. This isolation permitted the shell to be electrically biased either at cathode or keeper potential; the shell bias was selected by a switch external to the vacuum chamber.

Data obtained for these two configurations are shown in Figures 1 and 2. Figure 1 displays the dependence of anode-to-keeper voltage, V_δ, and beam current, I_B, on discharge propellant flow rate, $\dot{I}_{DHg}$, at fixed discharge current, I_D. This figure demonstrates the trend to increased V_δ and slightly reduced I_B for the shell-at-keeper-potential configuration when measured at fixed I_D and $\dot{I}_{DHg}$. Under these test conditions, this trend was clear from a decrease in the keeper voltage and slight increase in the discharge voltage and, consequently, increased V_δ. Also noteworthy in Figure 1 is a decrease in the highest obtainable beam current for the shell-at-keeper-potential configuration.

Figure 2 compares the performance data of both configurations by plotting discharge specific energy, ϵ_I, as a function of discharge propellant utilization efficiency, $\eta_{\dot{H}g}$. Data in this figure exhibit a shift in the "knee" of the curve toward increased ϵ_I and decreased $\eta_{\dot{H}g}$. These performance trends were also evident in the test results measured at I_D = 4.5 A, although the data are not displayed in Figures 1 and 2.

Our test results reproduced performance trends found in the original program. Since a net performance gain was not achieved with the shell at keeper potential, the shell was henceforth kept at cathode potential.

B. PROPELLANT-DIVERSION ENDPLATE

The thruster was reconfigured with a propellant-diversion endplate (Figure 3). The standard "dished" endplate was inverted, retaining a continuous magnetic circuit; the cathode polepiece was shortened, retaining discharge-chamber length and

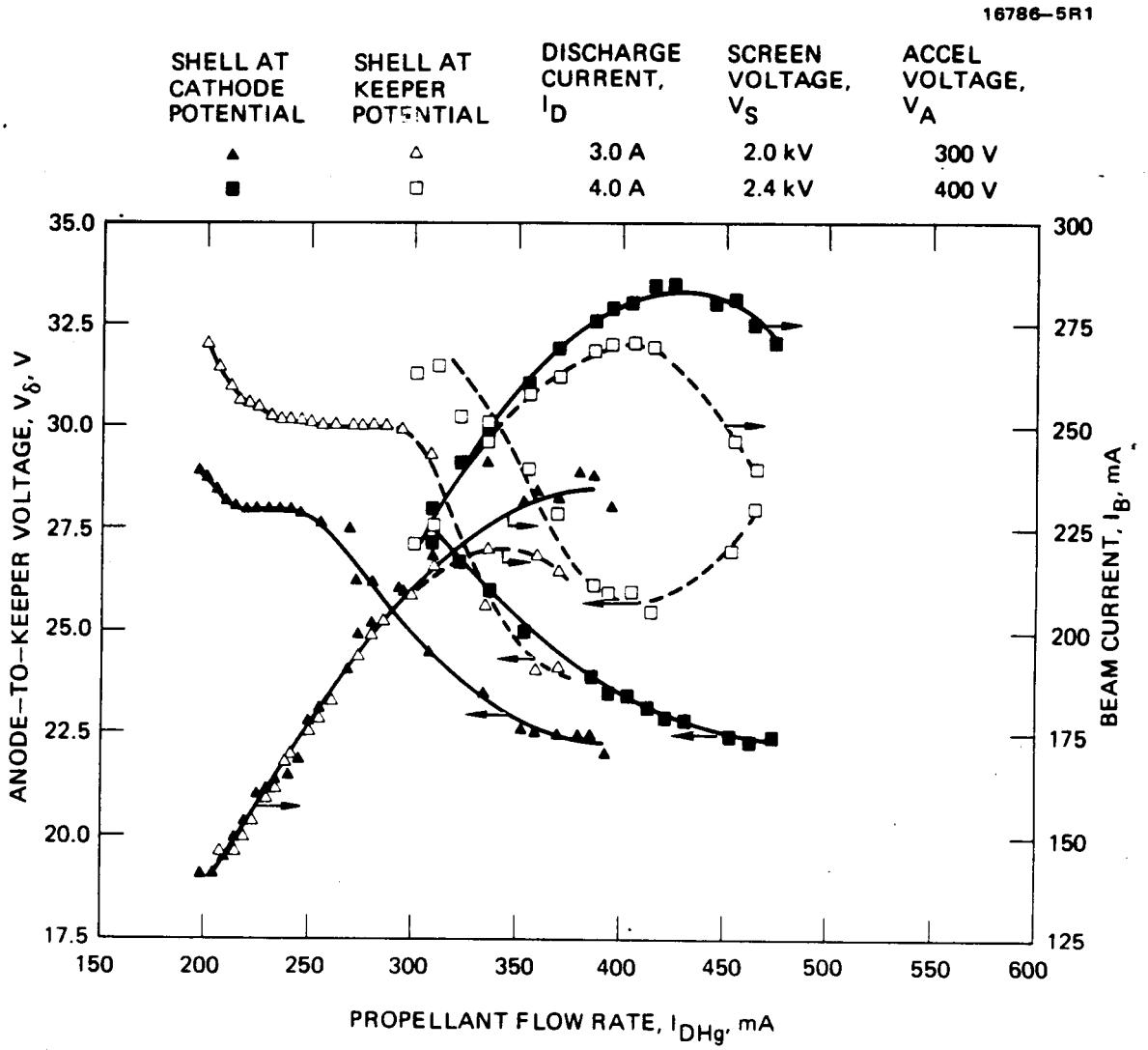

Figure 1. Propellant-diversion-endplate configuration: discharge-keeper voltage, V_δ, and beam current, I_B, as a function of propellant flow rate, I_{DHg}.

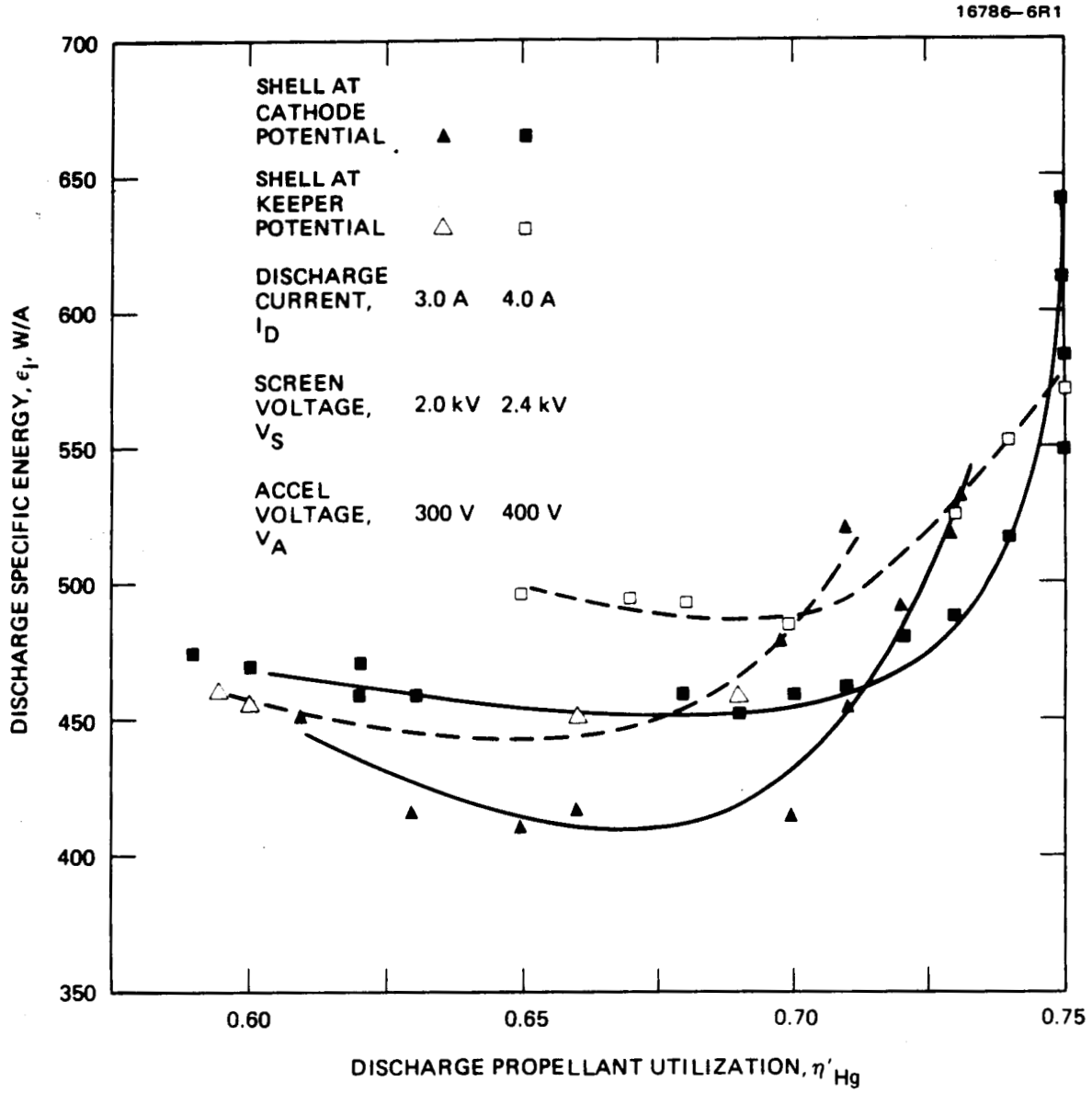

Figure 2. Propellant-diversion-endplate configuration: discharge specific energy, ϵ_I, as a function of discharge propellant utilization efficiency, η'_{Hg}

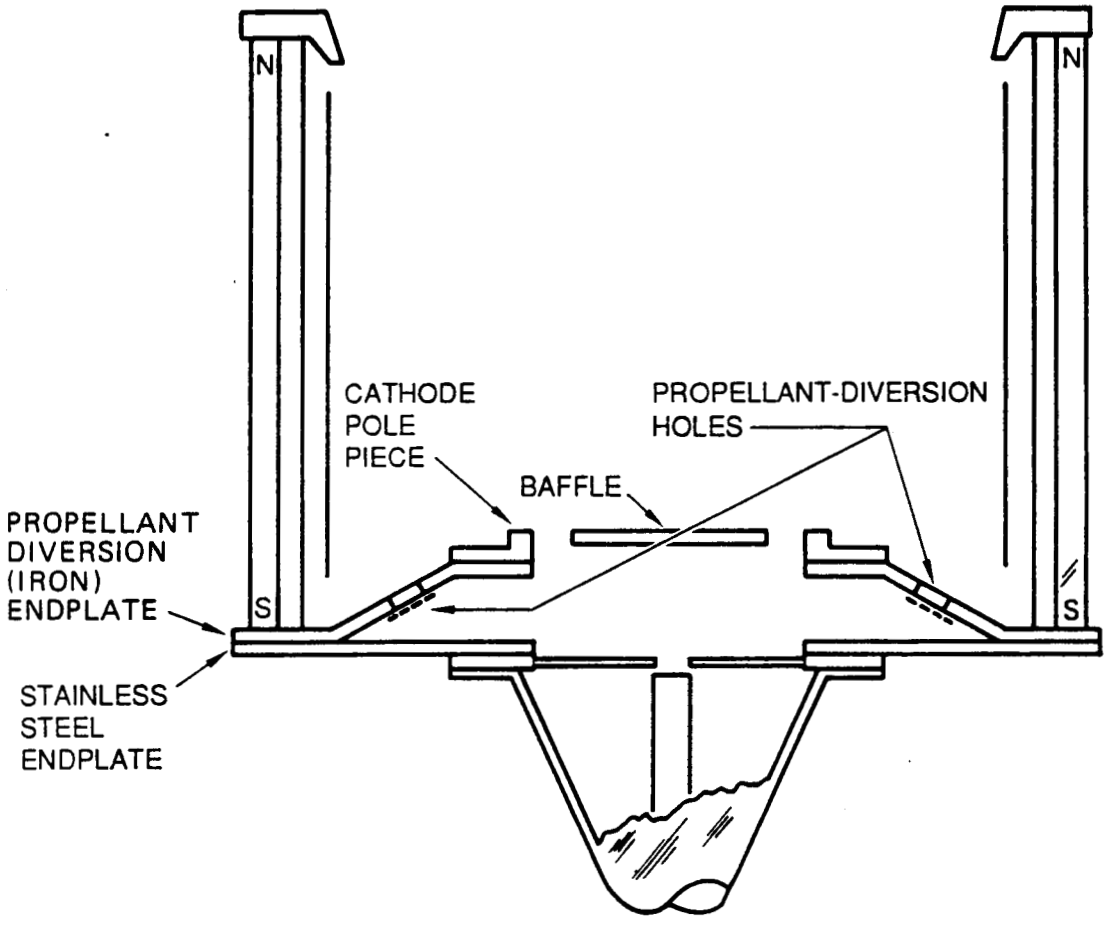

Figure 3. Propellant-diversion-endplate configuration: diagram of the propellant-diversion endplate configuration.

magnetic-field strength; and a flat stainless steel (nonmagnetic) endplate was installed to enclose the discharge chamber and support the cathode assembly. We provided propellant diversion by increasing the transparency of the endplate via wire-mesh-covered holes drilled through the inverted iron endplate. In some of our testing, a propellant-diversion baffle was also employed. This baffle, also tested in the original program, is perforated with three tantalum-mesh-covered apertures. These apertures redirect some propellant flow away from the baffle gap, without reducing plasma baffling.

Figure 4 displays performance data for three thruster configurations: (1) the propellant-diversion-endplate configuration with a 2.38-cm-diameter baffle, (2) a propellant-diversion endplate with a 2.38-cm-diameter propellant-diversion baffle, and (3) a standard IAPS configuration with the same baffle as in (2). Comparing these data indicates that configuration No. 1 gives the best performance, and configuration No. 2 the worst.

The data in Figure 4 demonstrate that there is an optimum degree of propellant diversion. These data indicate that propellant diversion increased the efficiency of propellant use (at I_D = 3 A) by approximately 20% to a value η'_{Hg} = 0.89, compared with a value η'_{Hg} = 0.69 for the standard configuration without propellant diversion (configuration No. 2). For these two designs the discharge specific energy remained essentially unchanged at a value $\epsilon_I \sim 425$ W/A. Such improvements confirmed the need for adequate propellant diversion at extended-performance conditions and demonstrated the simplicity of our approach.

C. SHORTENED DISCHARGE CHAMBER

We tested a configuration that reduces discharge chamber length. The length of the chamber was adjusted to a value two-thirds that of the standard IAPS discharge chamber. While

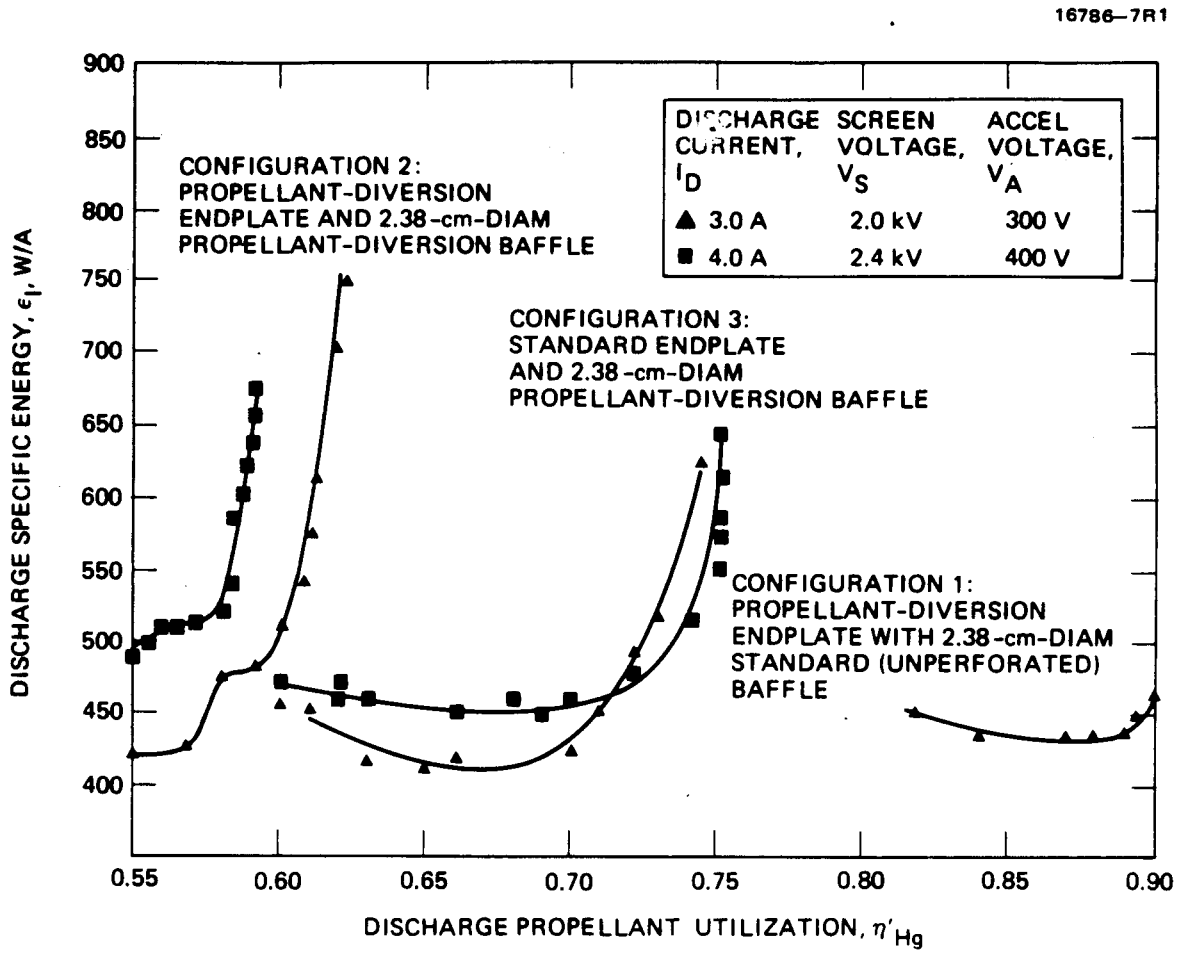

Figure 4. Propellant-diversion-endplate configuration: comparison of thruster performance curves.

testing this configuration, we found an unstable discharge over a range of discharge current I_D < 4 A and a discharge flow rate range of 200 mA < I_{DHg} < 550 mA. Although this instability was partially eliminated with a 5-Ω resistor connected in series with the discharge power supply, the shortened chamber was abandoned.

D. MAIN VAPORIZER AND PLENUM

We next modified the thruster by adding a vaporizer that supplied propellant to the discharge, independent of that supplied by the discharge vaporizer. Because this configuration exhibited the best performance obtained under this program, we refer to it as the "IAPS+" configuration. In this configuration (Figure 5), where the vaporizer is labeled "main" vaporizer, a gas plenum near the thruster endplate injects propellant into the discharge. The gas plenum was fabricated from 0.32-cm-diameter thin-wall stainless steel tubing formed into a circle. The downstream surface of the plenum was perforated with 36 holes, 0.51 mm in diameter, to distribute propellant uniformly into the discharge.

We employed the following techniques in evaluating the dual-vaporizer discharge chamber and thruster: the discharge current, I_D, and the discharge propellant flow rate, I_{DHg}, were fixed as the main propellant flow rate, I_{MHg}, was varied and thruster performance parameters were recorded. Table 1 lists the values of I_D, I_{DHg}, and I_{MHg} for these tests. Our results are displayed in Figure 6, where beam current I_B is plotted as a function of the ratio I_{MHg}/I_{DHg}. By comparing the values of the maximum beam current $I_B|_{MAX}$ (denoted by arrows) obtained at fixed I_D, we can determine the best range of values for the discharge propellant flow rate. The greater values of $I_B|_{MAX}$ are identified with the best thruster performance. In general, the best thruster performance occurs when the discharge-propellant flow rate is a small part of the main propellant flow rate. This characteristic (i.e., best performance with $I_{DHg} \ll I_{MHg}$) recalls that of the NASA/Hughes 30-cm thruster.

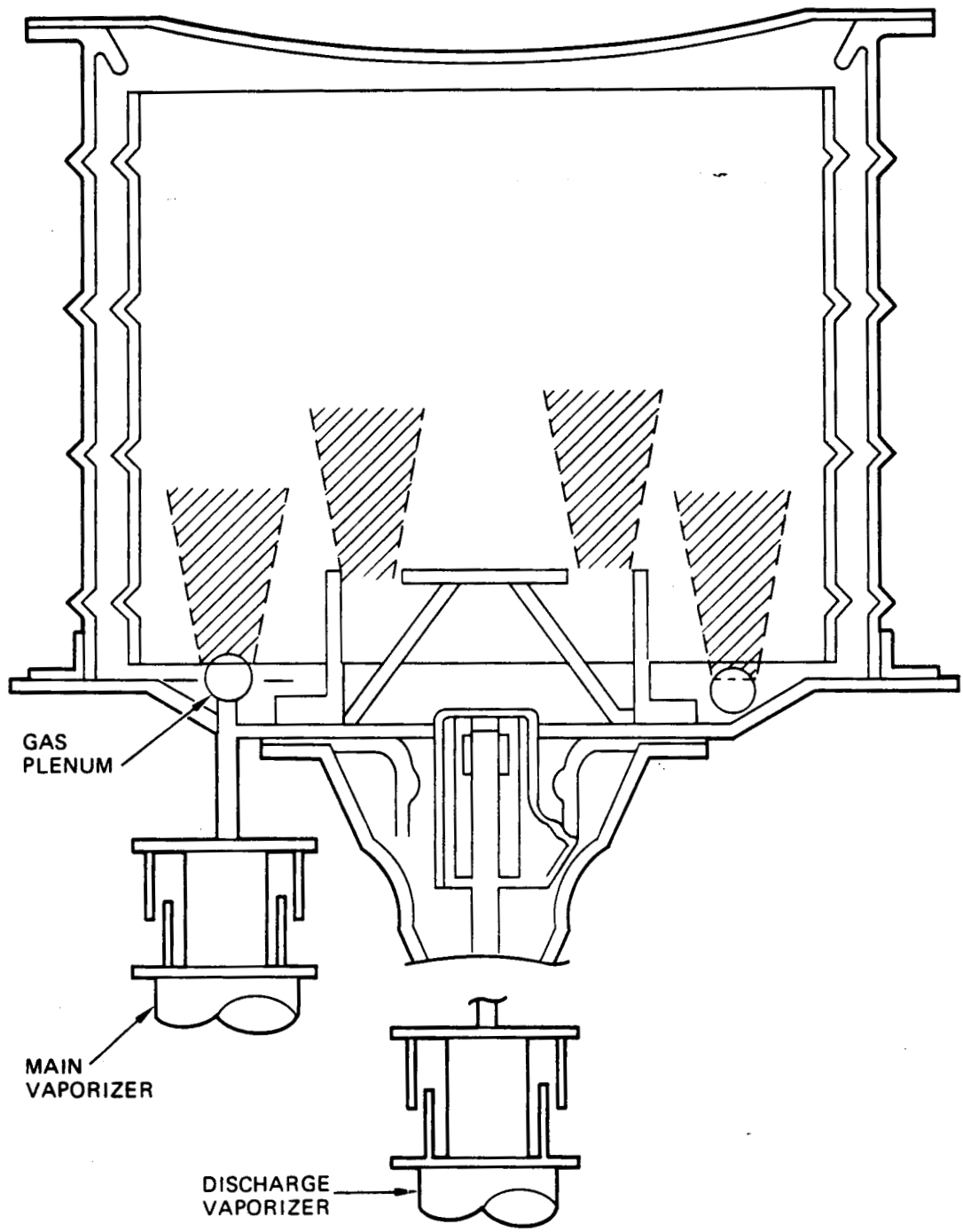

Figure 5. Diagram of the dual-vaporizer configuration.

Table 1. Test Conditions for Characterizing the Dual-Vaporizer Thruster

Discharge Current, I_D, A	Discharge Propellant Flow Rate, I_{DHg}, mA	Ratio of Flow Rates, I_{MHg}/I_{DHg}
1	39	2.43 to 3.27
	47	1.74 to 2.40
	81	0.35 to 1.12
	100	0.20 to 0.54
2	47	2.34 to 3.15
	76	1.49 to 1.89
	69	1.59 to 2.22
	165	0.20 to 0.37
3	47	4.8 to 4.94
	76	2.3 to 3.53
	116	0.97 to 1.97
	226	0.15 to 0.79
4	39	7.79 to 8.78
	44	6.79 to 8.78
	69	4.25 to 4.74
	95	2.34 to 3.58

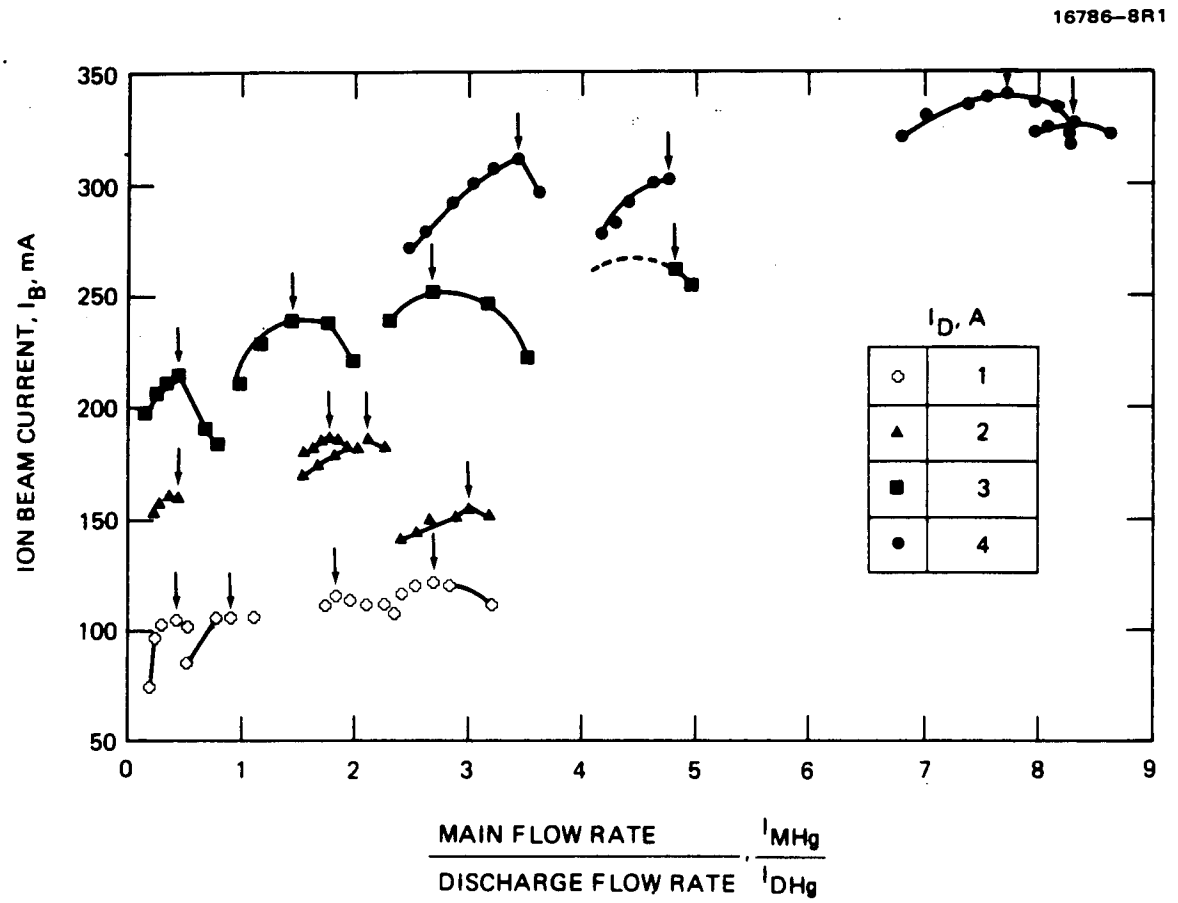

Figure 6. Ion beam current as a function of the ratio of main-to-discharge propellant flow rate for various discharge currents.

In controlling the 8-cm thruster or the 30-cm thruster at fixed discharge current, a decrease in the value of I_{DHg} increases the discharge voltage, V_D, without affecting I_B. An increase in $\dot{I}_{MHg}$ also increases the value of I_B without substantially affecting V_D. This result suggests that control loops like those in the 30-cm thruster can also be used in the dual-vaporizer 8-cm thruster.

In Figure 7, we plot ϵ_I versus η'_{Hg} for the four curves of Figure 6 displaying the best dual vaporizer performance. This figure shows the knee of the curve, for all values of I_D, occurring at the values $\epsilon_I \sim 350$ W/A and $\eta'_{Hg} \sim 0.9$. These data indicate that the thruster efficiencies represented by η'_{Hg} and ϵ_I are essentially constant over a wide range of discharge currents. In the baseline 8-cm thruster with a single vaporizer, the thruster performance decreases as the discharge current is increased; for example, at $I_D = 4.0$ A, the corresponding values are $\epsilon_I \sim 450$ W/A and $\eta'_{Hg} < 0.8$. Table 2 lists the thruster operating parameters measured at $I_B|_{MAX}$ and denoted in Figure 7 by arrows.

The data in Table 2 under the $I_D = 4.0$ A heading are the best obtained under this program for the IAPS+ thruster. However, we still performed one last test with a cathode-magnet assembly.

E. CATHODE-MAGNET ASSEMBLY

The use of a cathode magnet, which is diagrammed in Figure 8, was the last thruster modication test that we completed. In this design the cathode and keeper were located within the discharge chamber and surrounded by a cylindrical cathode magnet. This structure was composed of 12 paraxial magnets arranged in a ring around the cathode. The magnet array was terminated downstream in a magnetic polepiece that shaped the magnetic field near the cathode. This cathode-magnet arrangement resembles that used in the 30-cm-diameter ring-cusp thruster which recently demonstrated discharge specific energies in the

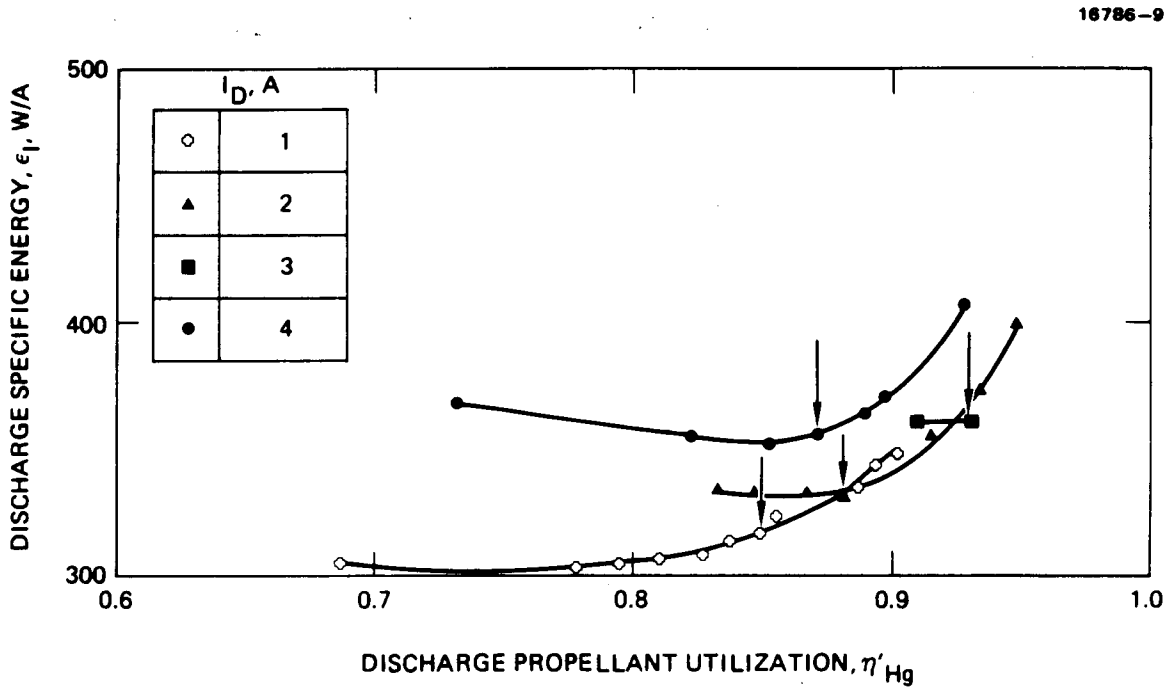

Figure 7. IAPS+ configuration: discharge specific energy as a function of discharge propellant utilization for various discharge currents that produce maximum beam current.

Table 2. IAPS+ Configuration Thruster Operating Parameters at $I_B|_{MAX}$

	Discharge Current, I_D			
	1.0 A	2.0 A	3.0 A	4.0 A
Discharge voltage, V_D (V)	37.6	31.0	31.3	29.8
Anode-to-keeper voltage, V_δ (V)	30	26.2	28.5	27.4
Discharge keeper current, I_{DK} (mA)	100	50	50	50
Discharge propellant flow rate, I_{DHg} (mA eq)	39	76	48	44
Main propellant flow rate, I_{MHg} (mA eq)	101	134	232	341
Screen voltage, V_S (kV)	1.2	1.5	2.0	2.4
Screen current*, I_S (mA)	120	187	261	338
Accel voltage, V_A (V)	-300	-300	-300	-400
Accel current I_A (mA)	0.7	1.3	1.5	1.9
Discharge specific energy, ϵ_I (W/A)	313	333	360	355
Discharge propellant utilization, η_{Hg} (%)	85	88	93	87
Specific impulse, I_{sp} (s)	2815	3254	3967	4062
Thrust, T (mN)	8	14	23	32

* For a given discharge current, parameters were adjusted to obtain the largest value of screen current; the values of I_s therefore correspond to $I_b|_{max}$.

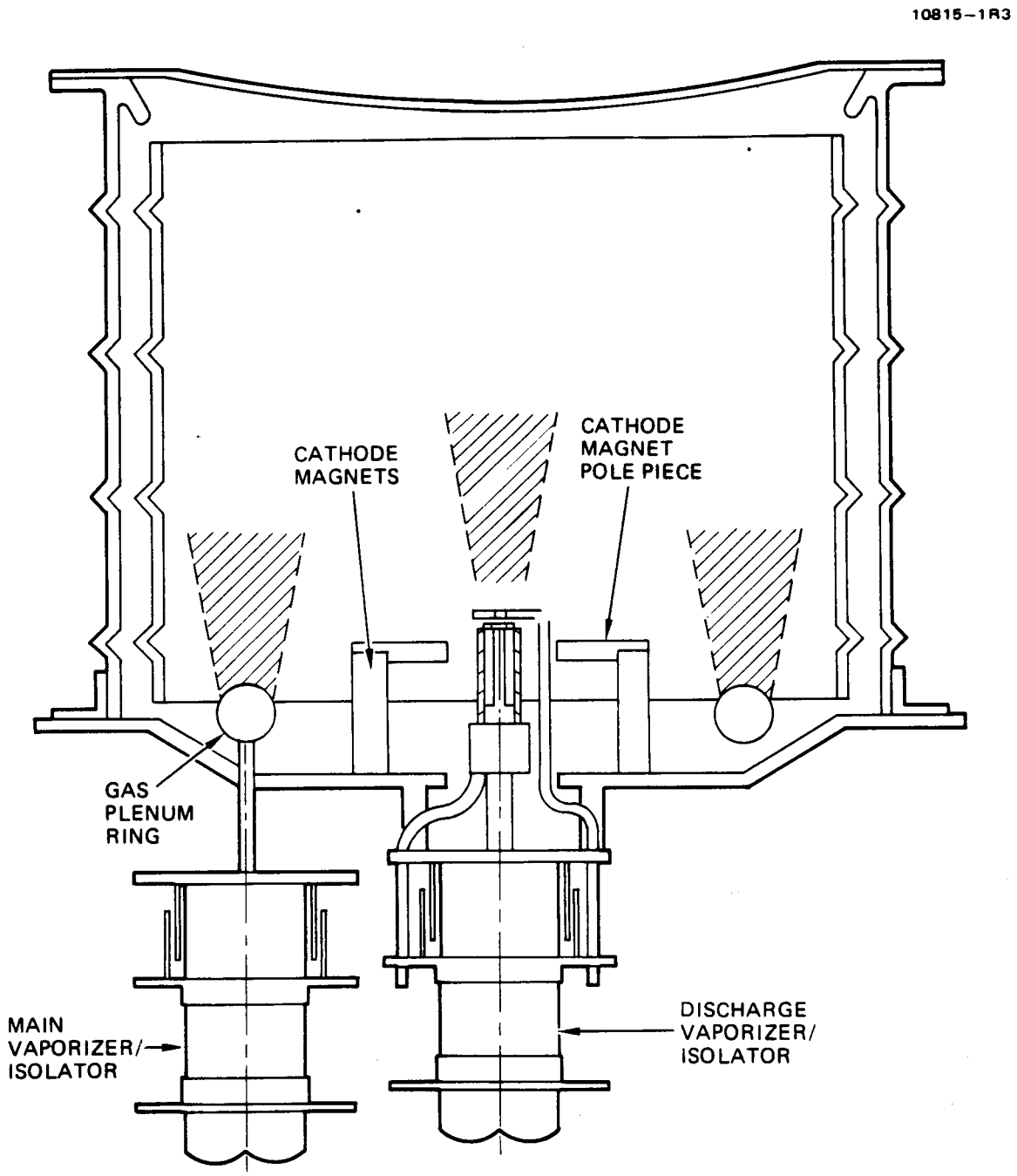

Figure 8. Diagram of the cathode-magnet configuration.

ϵ_I ~ 100 W/A range. The 8-cm thruster, however, does not share the 30-cm thruster features of a high-field-strength ring-cusp geometry.

Figure 9 compares performance curves of ϵ_I versus η'_{Hg} for both the cathode-magnet thruster and the IAPS+ thruster (described in Section 2-D). This figure indicates that performance in the cathode-magnet configuration declined when compared with that of the IAPS+ configuration. Nevertheless, our first effort with this cathode-magnet configuration might benefit from design revision. Table 3 compares the performance parameters for the IAPS+ and cathode-magnet thrusters.

Table 3. Performance Comparison of the IAPS+ and Cathode Magnet Configurations

Performance Parameter	IAPS+	Cathode Magnet Configuration
Thrust, T	32 mN	17 mN
Specific impulse, I_{sp}	4062 s	3484 s
Total input power, P_T	970 W	520 W
Total thruster efficiency, η_T	68%	59%
Discharge propellant utilization efficiency, η'_{Hg}	87%	82%
Discharge specific energy, ϵ_I	350 W/A	430 W/A
Thrust-to-power ratio, T/P	33.0 mN/kW	32.7 mN/kW

SUMMARY

Our work has shown that the best performance (Table 2, I_D = 4.0 A) is obtained with the following:

- IAPS+ thruster
- Shell at cathode potential

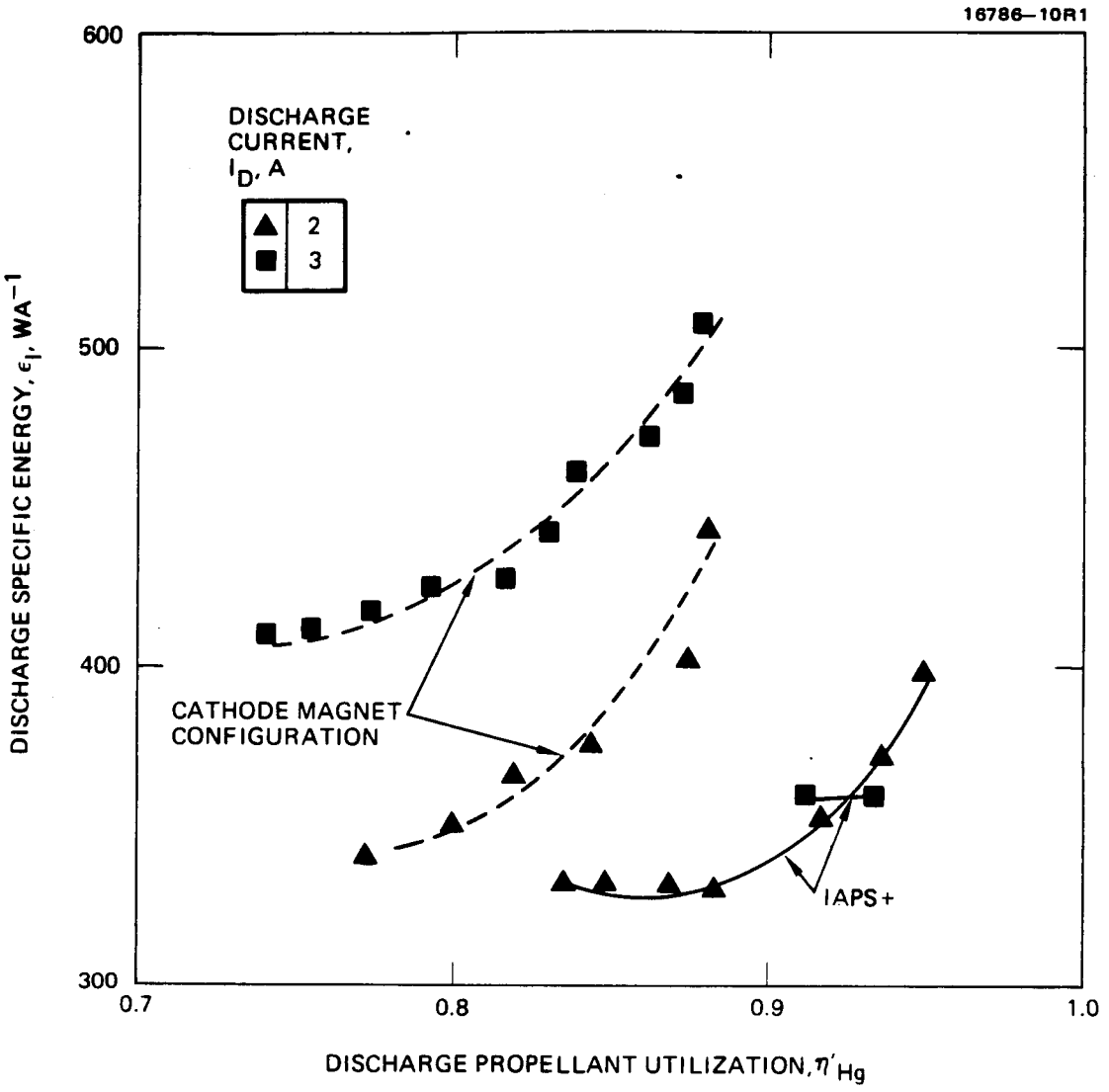

Figure 9. Performance curves of ϵ_I versus η'_{Hg} for the cathode-magnet and IAPS+ thrusters.

- Standard discharge chamber
- Standard baffle
- Additional plenun and vaporizer.

These results were presented in November 1982.[3] A detailed account of the thruster performance obtained under the original contract is available in a separate report.[1]

Following the thruster improvements described here, we investigated the simplified power processing unit.

SECTION 3

SIMPLIFIED POWER PROCESSING

We have designed a simplified power-processing unit (SPPU) for the 8-cm mercury ion thruster. Compared with the existing power-processing unit (PPU) used in the NASA/Hughes Ion Auxiliary Propulsion Subsystem (IAPS), this SPPU design provides a tenfold reduction in parts count, a decrease in system mass and cost, and improved reliability.

In this section, we discuss the design considerations underlying the SPPU design. We present specific thruster-control and thrust-level accuracy requirements that allow redesign of the PPU power supplies and control electronics for relaxed power-supply regulation and passive-control techniques. A modular approach to power-supply design further reduces the overall SPPU complexity. In addition, our method allows for a single power-supply design in all current-regulated power supplies with only slight component variations. In the remainder of this section, we describe a typical PPU subsystem, review the thruster-control requirements and previous simplification concepts, present the specific techniques employed to simplify the PPU, and discuss its use with an 8-cm thruster.

A. THRUSTER-CONTROL REQUIREMENTS

The operating and control requirements of all ion-thruster subsystems are highly similar: the larger-diameter thrusters, besides operating at greater power levels, require extra levels of PPU control due to the design necessity of an extra propellant injector and discharge-impedance adjustment. For simplicity, the discussion will be limited to the characteristics and requirements of the 8-cm mercury ion thruster.

The PPU controls the entire subsystem operation and contains the functional subunits displayed in Figure 10. It consists of a

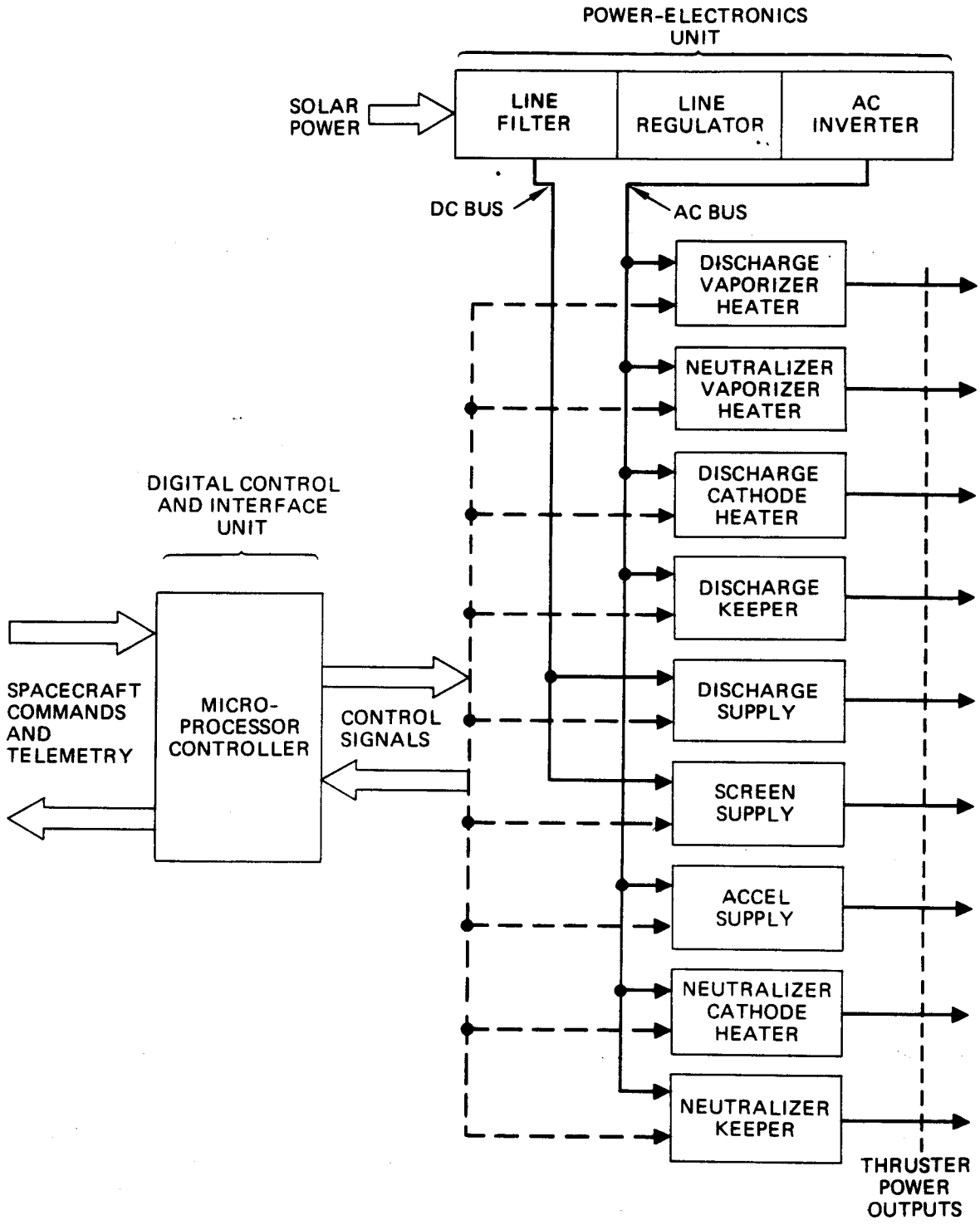

Figure 10. Functional block diagram of the 8-cm IAPS PPU.

Digital Control and Interface Unit (DCIU), and a Power Electronics Unit (PEU). The PPU conditions and regulates the solar-array power and supplies precisely controlled power to the thruster for propellant flow, ion generation, ion-beam acceleration, and ion-beam neutralization. The DCIU sequences and controls the output power of the PEU for thruster **ON, IDLE,** and **OFF** conditions. The DCIU also corrects abnormal thruster operating modes, provides telemetry signals indicating the status of each thruster power supply and gimbal orientation, implements ground-station telemetry for revised thruster operation, and drives the thrust-vectoring gimbal.

To achieve such control, the PEU is comprised of nine independent thruster power supplies, each of which is controlled by the DCIU. Table 4 displays the characteristics of the power supplies used in the existing IAPS 8-cm thruster subsystem PEU. Each power supply has multiple operating setpoints and highly regulated output power. The DCIU is a microcomputer that stores the thruster-control algorithms in read-only memory and contains random-access memory to store ground commands, thereby allowing modification of the thruster-operating characteristics.

The IAPS power-processing approach accommodates the experimental goals of the IAPS mission; these goals require a high level of system flexibility and the capability to regulate thrust with high precision. Because of these requirements, the IAPS PPU is highly complex and has a large parts count. For actual stationkeeping application, however, this level of flexibility and precision is not needed. The simplifications that we describe in the following sections address the considered elimination of those features of the IAPS PPU that would be unnecessary in a future workhorse-thruster environment.

1. Simplification of Power Processor Unit

To simplify the interface requirements, various approaches have been suggested, including extending the thruster performance

Table 4. Power Supply Specifications of the IAPS 8-cm Mercury Ion Thruster PPU

Supply	Function	Nominal Power	Regulation Type and ±%	Type Control
1. Discharge vaporizer heater	Propellant Flow	5 V at 2 A	I, 5	8 setpoints and loop control with D/A variable reference
2. Neutralizer vaporizer heater		2 V at 1 A	I, 5	Variable reference and loop control with D/A variable reference
3. Discharge cathode heater	Ion Generation	6 V at at 3 A	I, 5	8 setpoints
4. Discharge keeper		15 V at 0.36 A	I, 3	4 setpoints
5. Discharge		40 V at 0.5 A	I, 3	D/A variable reference
6. Screen	Ion Beam Acceleration	1180 V at 0.072 A	V, 1	Single setpoint
7. Accel		-300 V at 0.001 A	V, 1	Single setpoint
8. Neutralizer cathode heater	Ion Beam Neutralization	6 V at 3 A	I, 5	8 setpoints
9. Neutralizer keeper		20 V at 0.36 A	I, 3	4 setpoints

to reduce the number of thrusters and, hence, the number of PPUs required for a given mission[4]; reducing the number of thruster-power supplies by multiplexing a single power supply to perform multiple power functions[5]; relaxing the requirements on power-supply regulation to expand the range of circuit designs that may be used for simplification[6]; and eliminating unnecessary thruster-control loops.

If a decrease in thrust-system flexibility is acceptable, a major reduction in the interface-control requirements is possible by minimizing the number of operating setpoints and eliminating unnecessary control loops. Ideally, an ion thruster should be operated in two modes: **OFF** and **ON**, as in chemical propulsion. This approach would eliminate the requirement for variable output-thrust levels and reduce the power-supply control requirements. Table 5 lists the controls that we believe are needed in a simplified thrusting environment; we have successfully incorporated this control scheme into the SPPU. As shown there, all feedback loop control is eliminated and the power-supply setpoints are reduced to simple **ON/OFF** and **START/RUN** control. In this approach, a stable **ON** condition is reached by sequencing the thruster power supplies as one would in manual operation of a baseline thruster.

Another way of simplifying control requirements is to eliminate digital command of analog control loops. Digital commands used in the IAPS subsystem require a high electronic parts count because of analog-to-digital (A/D) and digital-to-analog (D/A) signal processing.

We can simplify the interface-power needs by relaxing the power-supply regulation (and ripple) requirements and by utilizing integrated circuits and state-of-the-art power-supply designs. The need to maintain stable thruster operation within a

Table 5. Simplified Power-Supply Control Requirements

Power Supply	Operating Control
Main-propellant flow	ON/OFF temperature
Discharge-propellant flow	START/RUN/OFF temperature
Discharge-cathode heater	START/RUN/OFF
Discharge keeper	ON/OFF
Discharge	ON/OFF
Screen	ON/OFF
Accel	ON/OFF
Neutralizer-propellant flow	START/RUN/OFF temperature
Neutralizer-cathode heater	START/RUN/OFF
Neutralizer keeper	ON/OFF

predetermined level of thrust accuracy determines power-supply regulation. This is illustrated by examining the thrust equation for an ion thruster:

$$T = 1.44 \times 10^{-4} \, I_B \, (V_B M_P)^{1/2} \quad ,$$

where

- T = Thrust, mN
- I_B = Ion beam current, A
- V_B = Beam voltage, V
- M_P = Propellant atomic mass, AMU.

To maintain a given thrust-level accuracy, I_B and V_B must be regulated within certain limits. These limits are translated

into design requirements for the power supplies which directly affect the values of these thrust parameters. In chemical-thrust systems, the beginning-of-life (BOL) to end-of-life (EOL) thrust variation can approach or exceed 10% of the BOL value. By comparison, conventional ion-thruster subsystems can maintain a thrust level within 1% of the BOL value for the rated ion-thruster lifetime (typically $\geq$10,000 h). By analogy with chemical propulsion, the thrust accuracy of ion thrusters can be reduced considerably.

After thruster testing and performance evaluation, we have established that 8-cm thruster systems will perform well with the reduced power supply requirements presented in Table 6. Reducing the thrust accuracy and regulation requirements also permits a wider range of circuit designs and electronic components. For a circuit design used in the 8-cm thruster simplified power-processor unit (SPPU), see the current-regulated circuits shown in Figure 11. The ac circuit [Figure 11(b)] is energized by a 20-kHz square wave input signal and contains a series impedance, Z, larger than the load impedance, Z_{load}. Therefore, the load impedance can vary over a wide range without significantly affecting the regulated current, I. This is illustrated by considering the circuit equation for this design,

$$I = \frac{V_{input}}{Z + Z_{load}}$$

If, for example, V_{input} = 100 V, and Z = 90 Ω = 10 x Z_{load}, then for a 100% variation in Z_{load}, Z_{load} = 10 Ω • 10 Ω, the circuit current will vary by only 10%, I = 1.0 A ± 0.1 A.

As an example of a voltage regulated supply, the voltage-regulated circuit (Figure 12) is energized by a dc input voltage and is actually a dc-dc inverter. This inverter achieves voltage regulation by pulse-width modulating the transformer primary drive power. Modulation occurs when we maintain a constant

Table 6. Simplified Power Processor Power Supply Requirements

Power Supply	Voltage	Current	Regulation, ±%	Set Points	Control
Discharge cathode heater	10 V	1 A, 5 A	20	2	Fixed
Discharge keeper	200 V/15 V	0.25 A	20	1	Fixed
Discharge	60 V/25-35 V	0 to 5 A	1	Variable	
Accel	-800 V	5 mA	10	1	Fixed
Screen	2.5 kV	300 mA	20	1	Fixed
Neutralizer keeper	200 V/15 V	0.5 A	20	1	Fixed
Neutralizer cathode heater	10 V	1 A, 5 A	20	2	Fixed
Neutralizer vaporizer heater	10 V	0.5 A, 5 A	5	2	Fixed
Discharge vaporizer heater	10 V	0 to 5 A	5	Variable	

13114-3R2

a. PASSIVE CURRENT REGULATION – DC

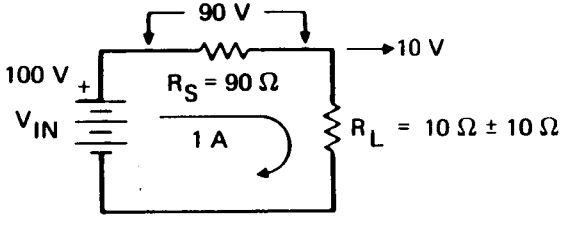

POWER TO LOAD = 10 W

POWER LOSS IN SERIES RES (R_S) = 90 W

$n = \frac{10}{100} = 10\%$

R_L	I
0 Ω	1.1 A
10 Ω	1.0 A (NOMINAL)
20 Ω	0.91 A

b. PASSIVE CURRENT REGULATION – AC

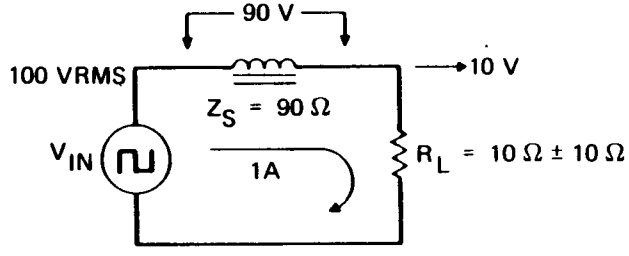

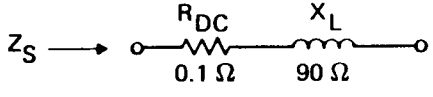

POWER TO LOAD = 10 W

POWER LOSS IN SERIES INDUCTOR (Z_S) ≤ 0.5 W

R_L	I
0 Ω	1.1 A
10 Ω	1.0 A (NOMINAL)
20 Ω	0.91 A

Figure 11. DC and ac open-loop passive regulation.

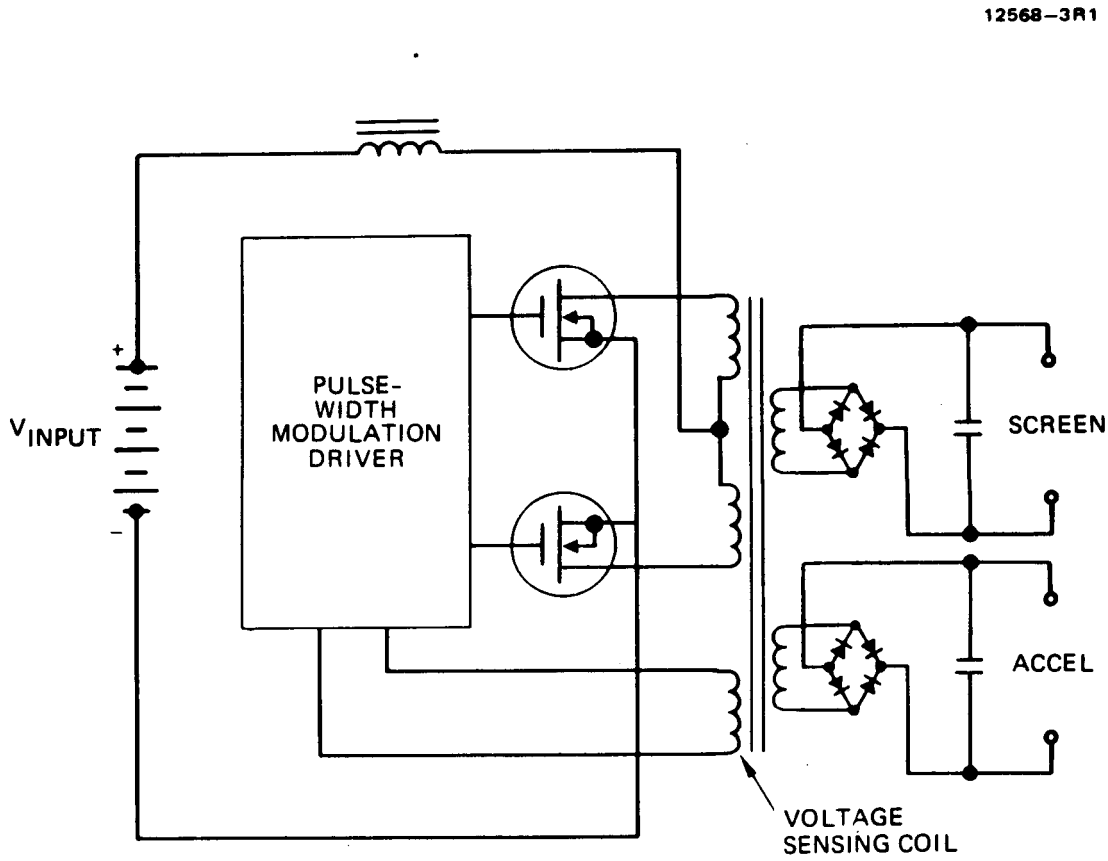

Figure 12. Circuit diagram illustrating simplification obtained by combining voltage-regulated supplies.

voltage across the voltage-sensing coil, a process which, in turn, tracks the voltage delivered to the load. In laboratory tests of this circuit, the output voltage varied by less than 5% for a 50% variation in the load impedance. This capability was achieved with a single integrated circuit which monitored the feedback signal and adjusted the pulse width of the drive transistors accordingly. The circuits shown in Figure 12 demonstrated efficiencies (output power divided by input power) that approached or exceeded 90%. Such efficiency compares favorably with that of existing power-processing practice.

Another approach to simplifying the PPU is to combine power supplies whenever possible, as the circuit in Figure 12 illustrates. The outputs of two or more power supplies (screen and accel) are combined onto a single drive transformer. When the output-power requirements track one another as they do for the screen/accel and cathode-heater/vaporizer-heater power supplies, this technique works well. Combining power supplies in this way further reduces the interface-control requirements, since a single control signal now regulates multiple-power outputs.

Since the screen supply controls about 70% of the entire SPPU output power and performs its own output regulation, the input power for the screen supply is derived directly from the solar panel bus voltage. This derivation reduces the power handling requirements of the housekeeping dc-dc regulator and dc-ac inverter and minimizes power losses in those supplies. Independently operating the screen supply also permits a much higher operating frequency to minimize the weight and size of the required magnetic and capacitive components. Isolated dc output power is supplied to provide both the 2500-V screen output and the 800-V accel output from the same output transformer. That transformer provides automatic tracking between the two supplies. Current limiting to protect against thruster shorts is provided by sensing the FET switch current and reducing the gate drive

pulse width to maintain safe peak current levels during the shorting interval. Controlled turn-on (soft start) can be accomplished in the same manner.

Another way to simplify the power supply is through a modular multipurpose circuit design requiring only simple adjustments in the power supply operating point or component substitution. This approach suits the current-regulated power supply designs and designs for thrusters of various diameters and power requirements. As presented in Table 4, a mercury ion thruster requires seven current-regulated power supplies for proper operation. These supplies can all be designed using the approaches shown in Figure 11. Three supplies – the discharge, discharge keeper, and neutralizer keeper – can be operated directly from the ac power source with no additional switching or control. The actual design requires only the addition of an isolation transformer, output rectifiers, and a filter capacitor to provide dc voltage. Figure 13 shows a typical detailed schematic of the circuit used for these three supplies.

However, discharge and neutralizer cathode heater and discharge and neutralizer vaporizer heater supplies all require some variable power, which requires a controllable ac switch. The block diagram of a typical variable-current-regulated supply is presented in Figure 14. The basic inductor-controlled, current-regulated technique described previously is used for these supplies with the additional capability to turn **OFF** the power. By switching the power **ON** and **OFF** at a relatively low rate (50 to 100 Hz) and controlling the duty cycle of the switch, any power level required by the thruster can be generated. As a result of the long thermal time constants of thruster heaters and vaporizers (several seconds), 50- to 100-Hz power pulses are quite effectively smoothed to provide an average dc power.

C16786-1

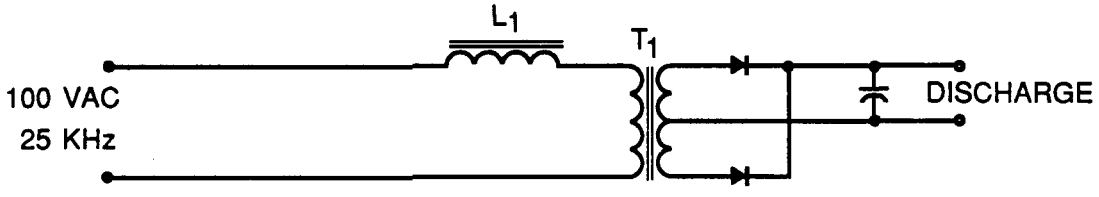

Figure 13. Typical fixed-current, current-regulated supply used for discharge, discharge keeper and neutralizer keeper supplies.

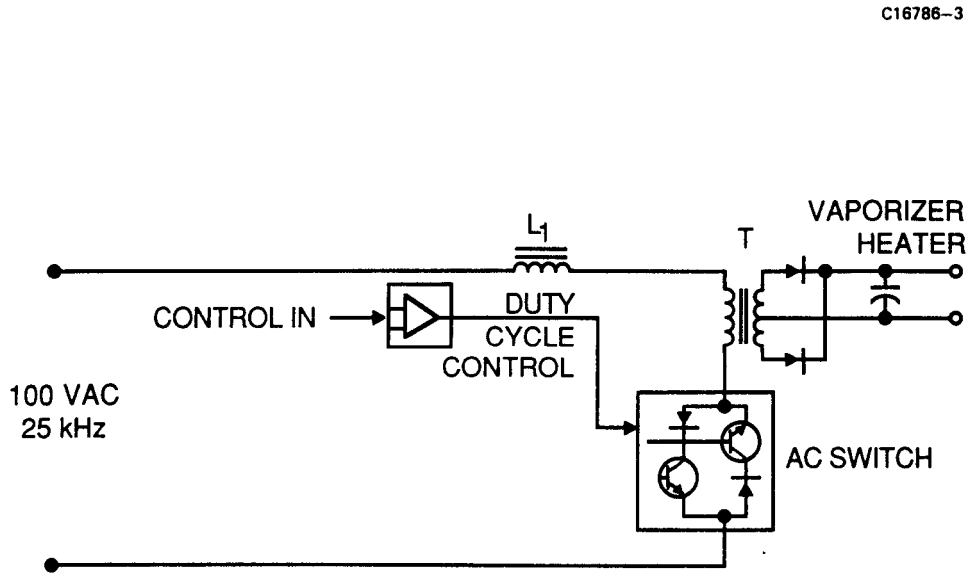

Figure 14. Typical variable-current, current-regulated supply used for discharge and neutralizer heater and vaporizer supplies.

2. Thruster Interface-Control Requirement

The power processor must interface between raw dc power obtained from the spacecraft energy sources – solar panels, batteries, or generators – and the required thruster operating load function. These thruster functions include propellant injection, ion generation and acceleration, and ion-beam neutralization. For these functions the power processor must sequence and adjust the various power supply outputs as demanded by the thruster dynamic operating conditions. Typical thruster functions and the supplies required to control those functions are listed in Table 7. These supplies must be controlled and sequenced in the proper order to start up and run the thruster very stably and efficiently. Table 8 illustrates the typical power-supply sequences required for such operation.

B. THRUSTER CONTROL AND SEQUENCING TECHNIQUES

1. Vaporizer Duty Cycle Operation

Vaporizer flow rate is controlled by sensing vaporizer temperature and adjusting the power to the vaporizer to maintain its temperature. The basic variable-current regulation technique described previously and shown in Figure 15 is used for supplying vaporizer heater power:

- Startup with high power (85% duty cycle) until **START** temperature is reached.
- Lower duty cycle to maintain **START** temperature.

Upon keeper ignition:

- Reduce **START** temperature to **RUN** temperature.
- Reduce (automatically) duty cycle to maintain **RUN** temperature.

The cathode heater is controlled with the same duty cycle modulation technique, except the **START** and **RUN** power levels are

Table 7. Typical Thruster Power-Supply Requirements

Operating Requirement	Power Supplies Required
Propellant injection	Neutralizer-vaporizer-heater supply Discharge-vaporizer-heater supply
Ion generation	Discharge-keeper supply Discharge supply
Ion acceleration	Screen supply Accel supply
Ion-beam neutralization	Neutralizer-keeper supply
Cathode or discharge ignition	Neutralizer-cathode-heater supply Discharge-cathode-heater supply

Table 8. Power-Supply Sequencing to Achieve Stable Thruster Operation

Initiate Plasma Discharges by Turning On:

- Neutralizer and discharge cathode heaters (initiate discharge ignition)
- Neutralizer and discharge-vaporizer-heater supplies (to start flow rates)
- Neutralizer and discharge keeper supplies
- Discharge supply

Stabilize Plasma Discharges by:

- Reducing neutralizer and discharge cathode heaters (to run levels)
- Reducing neutralizer and discharge-vaporizer-heater supplies (to run flow rates)

Extract Ion Beam by Turning On:

- Screen and accel supplies

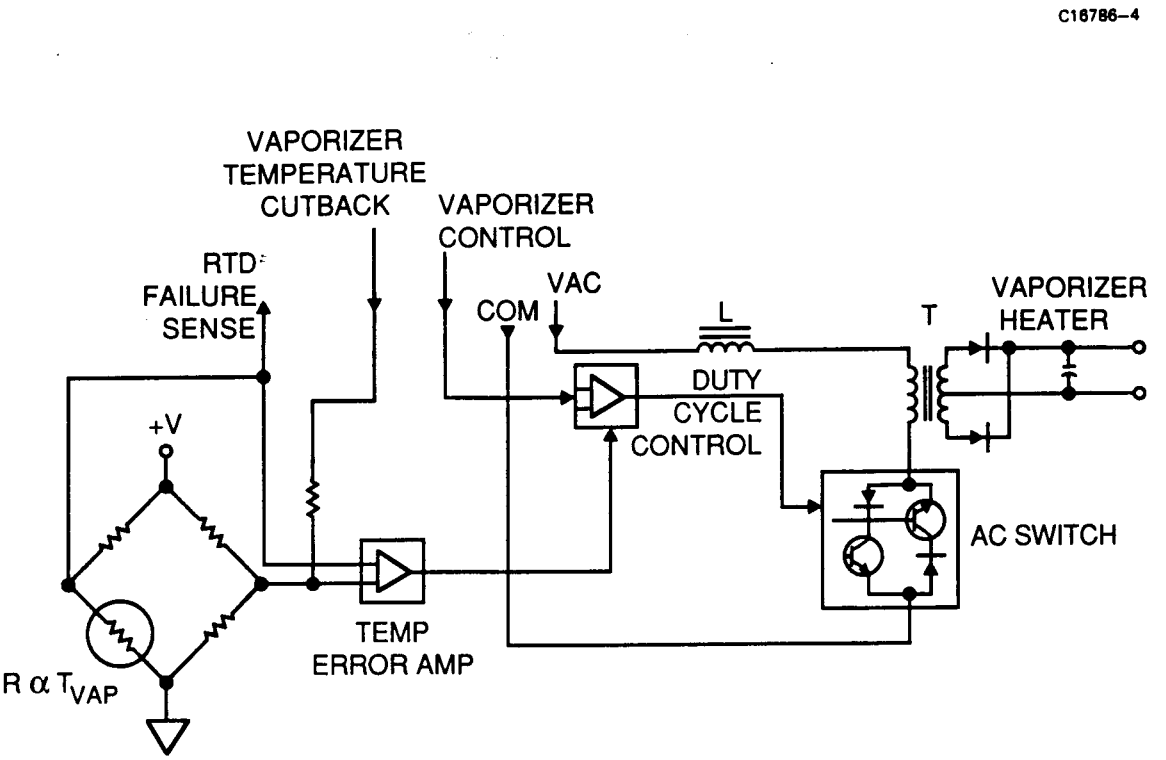

Figure 15. SPPU vaporizer heater power supply.

fixed power level set points. As with the vaporizer supplies, the power level, from start to run levels, is cut back upon keeper ignition.

High voltage power supplies (screen and accel) are maintained **OFF** until both keepers and the discharge have ignited and the discharge voltage has dropped below 50 V. The high voltage is then turned **ON** and slowly (0.5 s) ramped up to full voltage. If an overcurrent condition or plasma arc (short) occurs or one of the keepers extinguishes, the high voltage is automatically shut **OFF** and the high-voltage turn-**ON** sequence is repeated. The sequence will recycle continuously if a short is maintained on either high voltage supply.

2. Failed RTD Temperature Sensor Control Technique

If an RTD temperature sensor fails, the control circuitry switches to fixed-set-point or fixed-duty-cycle control. The set points are chosen under average conditions to give the required duty cycle for producing the **START** temperature during startup and the **RUN** temperature after keeper ignition.

Figure 16 shows the basic cathode-heater and vaporizer-heater control circuit used for both the discharge and neutralizer sections. Under normal conditions, the RTD acts as part of a bridge circuit, which produces outputs in the 1 to 3 V range. Modulator U_{2A} amplifies these signals and controls the duty cycle modulator U_{2C} which, in turn, controls the ac power switch. When an RTD fails, it becomes an open circuit and allows the bridge output to rise to 10 V, which disables modulator U_{2A} and closes the switch contacts x_2 and x_3 in U_1. The vaporizer duty cycle is then fixed at the levels set by R_{45} and R_{47}.

3. Keeper and Discharge Supplies

In addition to regulating the current, the two keeper supplies and the discharge supply must provide high voltage (~200 V) for igniting the plasma arc during the start phase. If

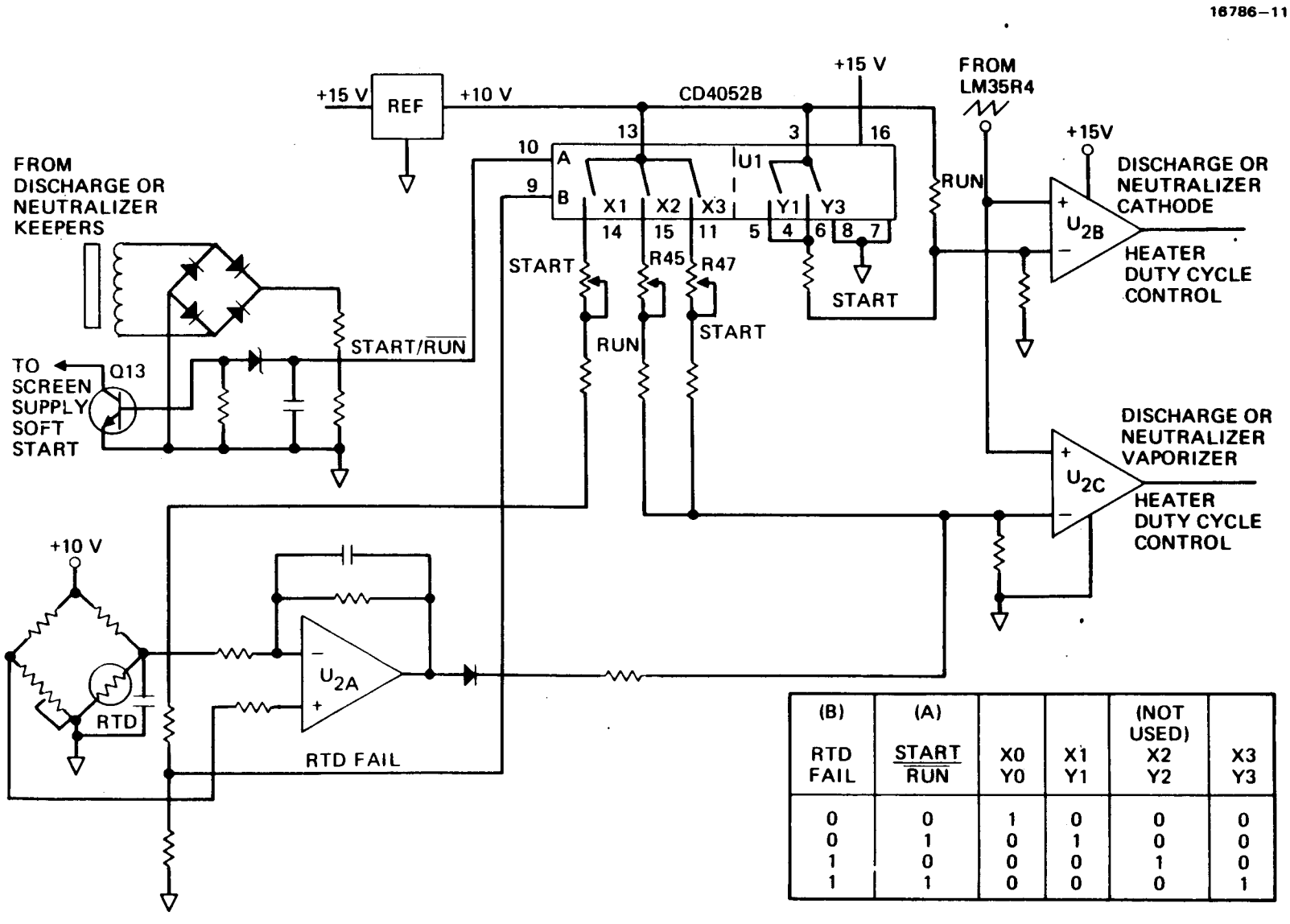

(B) RTD FAIL	(A) START/RUN	X0 Y0	X1 Y1	(NOT USED) X2 Y2	X3 Y3
0	0	1	0	0	0
0	1	0	1	0	0
1	0	0	0	1	0
1	1	0	0	0	1

Figure 16. SPPU-start and failed RTD control circuitry.

we use an output transformer with a 2:1 step-up ratio, the output voltage in the open circuit condition (typical keeper load before ignition), peaks to 200 V or more. After ignition, with keeper current flowing, the output voltage drops to a typical keeper voltage of 15 V because of the high series impedance exhibited by the current-regulating choke. If a keeper extinguishes, the keeper current goes to zero. The keeper voltage will automatically return to the high voltage state ready for re-ignition.

Figure 17 illustrates a complete SPPU system in block diagram form. Each major control line is identified (CL-1 through CL-12), and the analog control function with which it is associated is described. A more detailed analysis of each control loop is given in Table 9.

C. TEST RESULTS FOR THE 8-CM MERCURY-ION-THRUSTER SPPU

We designed and built a laboratory-type SPPU for the 8-cm-diameter mercury-ion thruster, incorporating all of the circuit topologies described above. This SPPU provided the power and control requirements for the 8-cm thruster and achieved our program goals:

- A one-switch, hands-off thruster startup.
- Automatic sequencing to stable operation when the thruster was started from a full **OFF** condition.

Tests were conducted under three conditions: (1) thruster at room temperature (T_{SHELL} = 23°C), (2) thruster at warm temperature (T_{SHELL} = 150°C), and (3) thruster at nominal operating temperature (T_{SHELL} = 300°C). These conditions simulated a limited range of potential thruster operating temperatures or environmental conditions. We demonstrated the capability for complete thruster control without any complicated software or digital commands (as used in the IAPS).

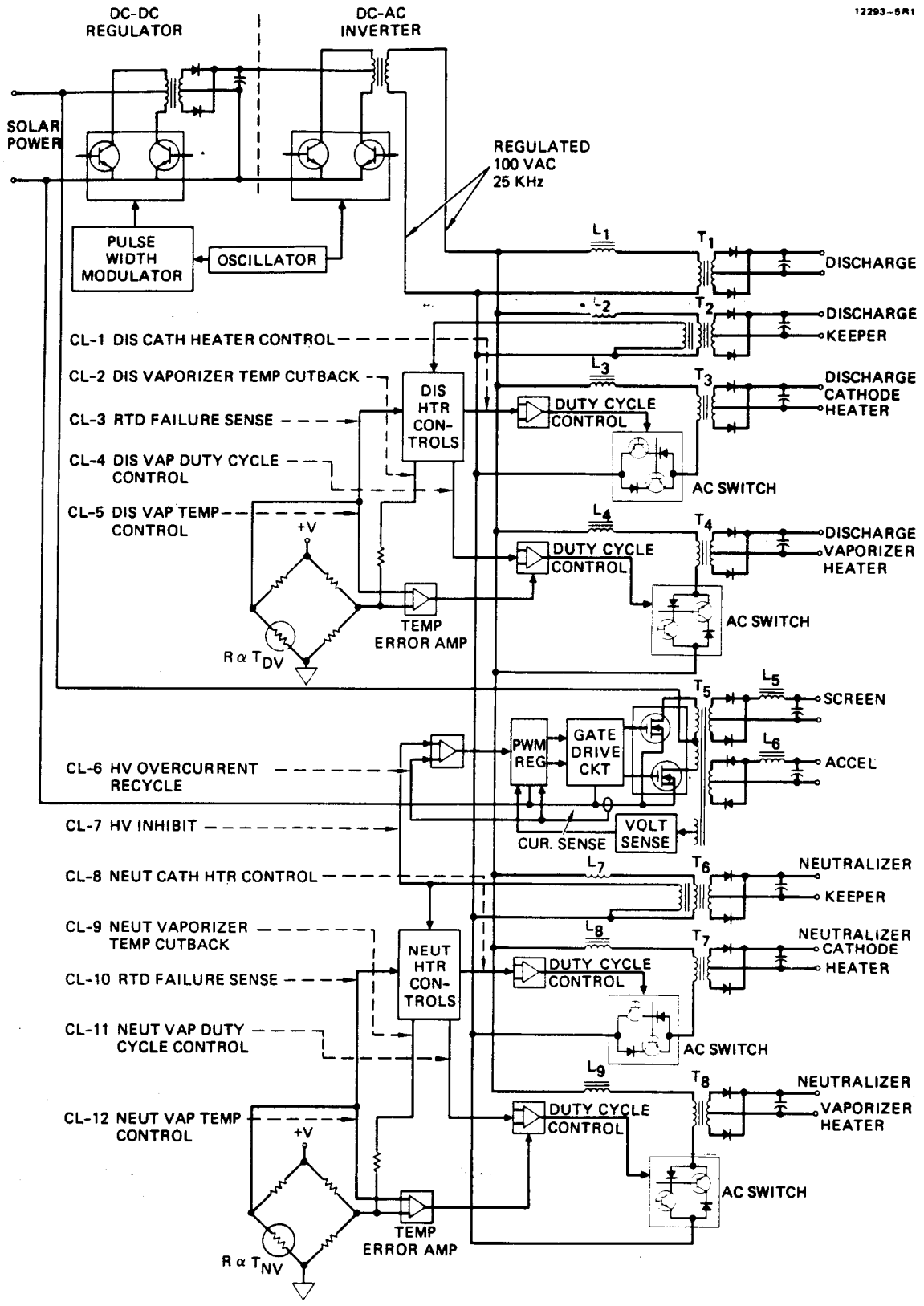

Figure 17. Schematic diagram of the simplifed power-processing unit (SPPU). (SPPU control functions CL-1 to CL-12 are defined in Table 9.)

Table 9. 8-cm SPPU Control Functions

CL-1	Discharge-cathode-heater power is switched from **START** duty cycle (~85%) to **RUN** duty cycle (~60%) upon discharge-keeper ignition.
CL-2	Discharge-propellant flow rate is switched from **START** flow rate to **RUN** flow rate upon discharge-keeper ignition.
CL-3	Upon RTD failure (open-circuit), the discharge-propellant flow power supply is switched from fixed temperature control to fixed duty cycle control.
CL-4	In failed RTD condition, the discharge-propellant flow power supply is switched from the **START** duty-cycle setpoint (~85%) to the **RUN** duty-cycle setpoint (~60%).
CL-5	The discharge-propellant flow rate is maintained at either the **START** or **RUN** flow rate by varying the duty cycle of the discharge propellant flow power supply.
CL-6	High-voltage supplies (screen + accel) are turned **OFF** momentarily if an overcurrent is sensed in either the screen or accel power supplies. High voltage is periodically turned **ON** to check whether the overcurrent condition still exists.
CL-7	High-voltage power supplies are turned **OFF** until the neutralizer keeper ignites following neutralizer keeper extinction.
CL-8	Neutralizer-cathode-heater power is switched from **START** duty cycle (~85%) to **RUN** duty cycle (~60%) upon neutralizer keeper ignition.
CL-9	Neutralizer propellant flow rate is switched from **START** flow rate to **RUN** flow rate upon neutralizer keeper ignition.
CL-10	Upon RTD failure (open circuit), the neutralizer-propellant flow power supply is switched from fixed temperature control to fixed-duty-cycle control.
CL-11	In failed RTD condition, the neutralizer-propellant flow power supply is switched from the **START** duty-cycle setpoint (~85%) to the **RUN** duty-cycle setpoint (~60%).
CL-12	The neutralizer-propellant flow rate is maintained at either the **START** or **RUN** flow rate by varying the duty cycle of the neutralizer propellant flow power supply.

The startup algorithm of the SPPU follows the power supply sequencing steps illustrated in Table 8. The response of the various thruster operating parameters during an idealized startup sequence is graphically presented in Figure 18 to illustrate the concepts of the startup algorithm.

As power is applied to the SPPU, all power supplies energize simultaneously (time = t_0 in Figure 18), except for the combined screen/accel supply. During this startup phase, the (neutralizer and discharge) cathode heaters and vaporizer-heater power supplies operate at ~85% of their maximum output power levels. This percentage is achieved by modulating the duty cycle of the various ac switches. Meanwhile, the discharge and (neutralizer/discharge) keeper power supplies go to their full open-circuit output voltage.

As the preset **START** temperatures of the vaporizers (discharge and neutralizer) are reached ($t = t_1 - \Delta$ for the neutralizer vaporizer and $t = t_2 - \Delta$ for the discharge vaporizer), the duty cycles of the ac switches are gradually reduced. This reduction limits the power delivered to the vaporizer heaters and maintains a fixed vaporizer (**START**) temperature.

As the keeper-plasma discharges ignite (at $t = t_1$ for the neutralizer keeper and $t = t_2$ for the discharge keeper), the duty cycles of the respective cathode-heater and vaporizer power supplies are immediately reduced to preset **RUN** values. Such values limit the supply outputs to about 60% of their maximum output power levels. This reduction in output power lowers the vaporizer temperatures to the **RUN** values required for optimal thruster performance.

Following ignition of the discharge keeper, the discharge current increases, resulting in a fully established discharge plasma and a gradually decreasing discharge voltage. When a preset discharge voltage is reached (typically 50 V), the combined screen/accel power supply energizes and the ion beam is extracted. If either of the keepers extinguish, the screen/accel

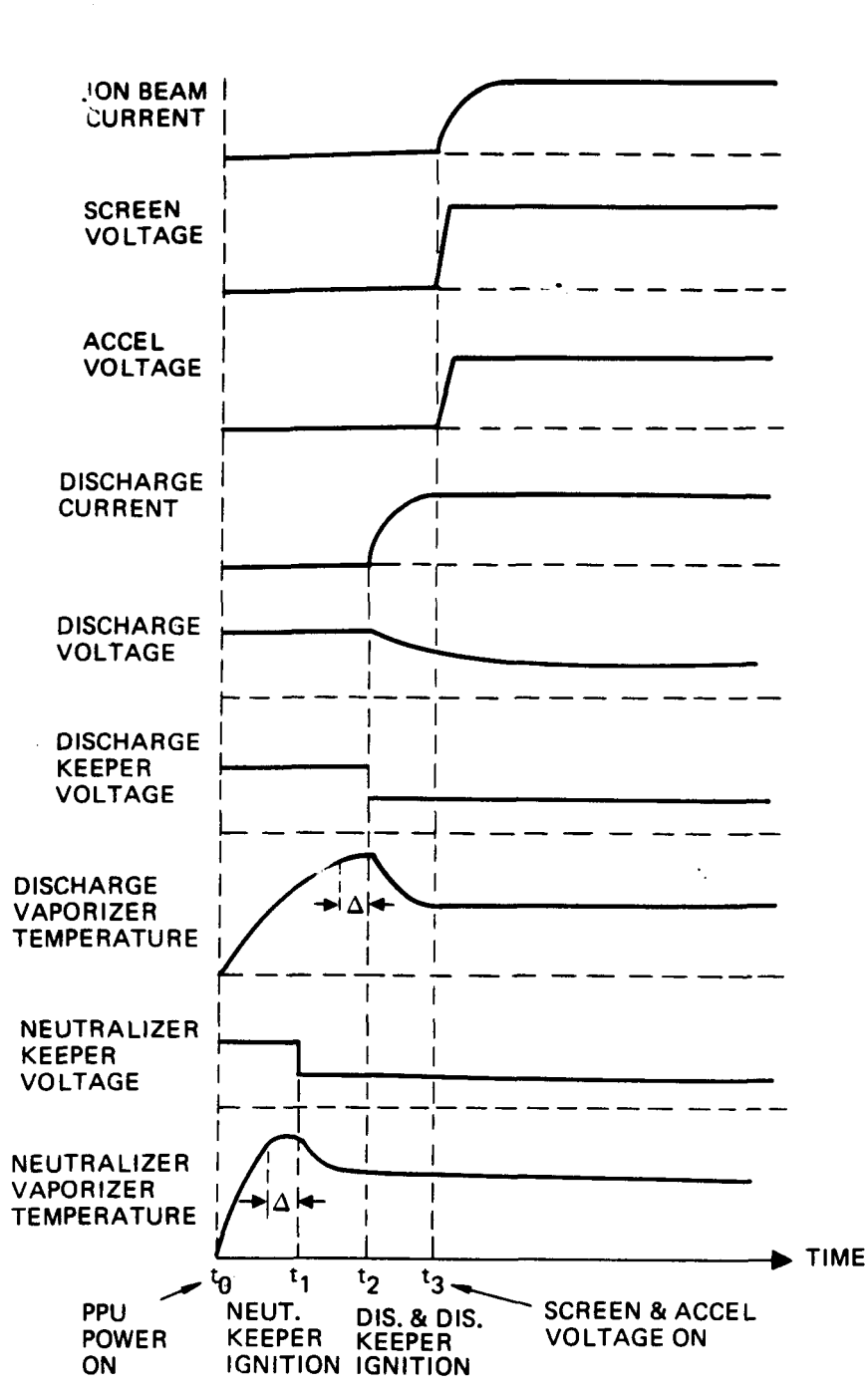

Figure 18. Idealized thruster startup sequence with the SPPU.

power supply is immediately turned **OFF** and inhibited until the (keeper) discharges are reestablished. This combined screen/accel power supply is also turned **OFF** and recycled in case an overcurrent condition occurs in the ion-extraction electrodes.

Starting with the thruster shell at room temperature (T_{SHELL} = 23°C), the transition to maximum-ion-beam conditions was achieved within 10 min, following application of power to the SPPU.

With the thruster shell at normal operating temperature (T_{SHELL} = 300°C), the transition to maximum ion-beam current was achieved within 5 min. This temperature dependence is a common characteristic of mercury thrusters (as opposed to inert-gas thrusters): during startup, cold surfaces within the thruster cause mercury vapor to condense; as the thruster-shell temperature increases, the propellant reevaporates. The net effect of propellant condensation is a brief period of inefficient ("flooded") thruster operation. This problem is avoided in inert-gas thrusters since commonly used inert-gas propellants (argon, xenon, and krypton) do not condense at temperatures typical of the space environment. Figure 19 records pertinent thruster parameters during an actual startup sequence (as opposed to the conceptual sequence illustrated in Figure 18).

The overall simplicity of our SPPU design is illustrated by comparing the parts count for this unit with that of the PPU in the present 8-cm IAPS thruster subsystem. Table 10 displays the parts count for the various subsections of these two power-processor units. As illustrated, we reduced the number of electronics parts by a factor of ten. The parts count attributed to the remaining two subsections of telemetry/power conditioning and filtering are only estimates for the SPPU, since these subsections were not made or installed in the SPPU hardware described here. Based on our arguments for three channels of telemetry and our circuit designs for power filtering/conditioning applications, these estimates demonstrate the potential parts

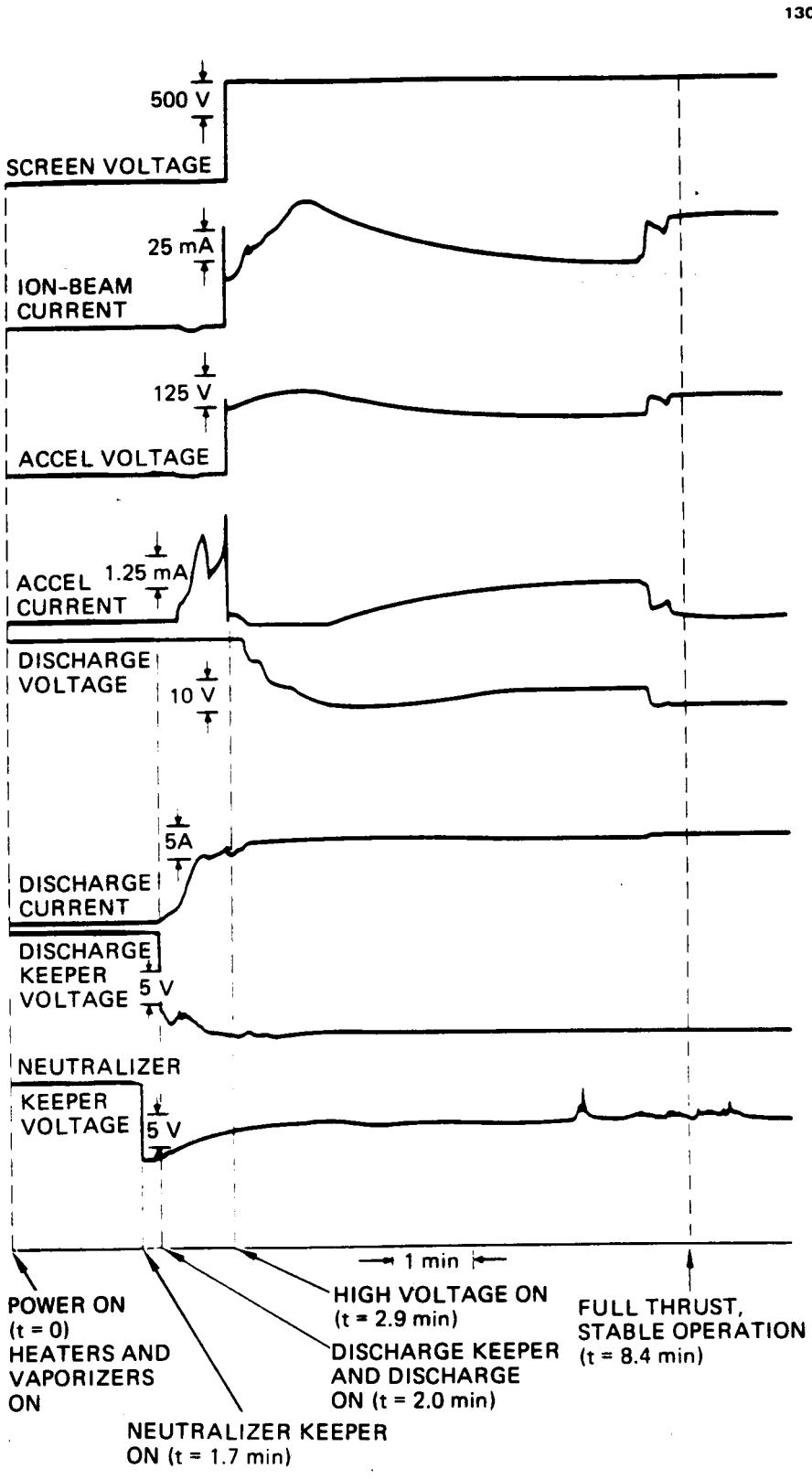

Figure 19. Actual thruster startup sequence with SPPU, beginning at ambient room temperature (~300 K).

count reduction for a "complete" SPPU. Compared with the IAPS PPU, our SPPU has a factor of ten fewer parts. A discussion of the preceding results is included in an AIAA paper.[7]

Table 10. Parts Count Comparison for the 8-cm IAPS PPU and SPPU Designs

Subsection	Approximate Parts Count	
	IAPS PPU	SPPU
Power electronics	1690	174
Telemetry	238	36
Power filtering and conditioning	367	50
Total	2295	260

SECTION 4

CONCLUSIONS

In this Supplemental Final Report, we have:

- Characterized the baseline 8-cm IAPS thruster
- Incorporated modifications to extend the performance capabilities of the 8-cm IAPS thruster
- Characterized the modified 8-cm thruster
- Simplified the IAPS PPU.

Prior to the modifications described in this report, the maximum IAPS thruster performance was determined to be T = 17 mN, I_{SP} = 2300 s, and I_B = 0.215 A. By incorporating a plenum and second vaporizer, we increased performance to T = 32 mN, I_{SP} = 4062 s, and I_B = 0.310 A. We believe the IAPS thruster can be upgraded to operate at higher thrust levels. Although testing a cathode magnet did not improve the thrust levels, we feel that another design might further improve the performance.

We have dramatically simplified the PPU design and parts count while retaining essential subsystem control over the thruster operation. Our design for a simplified power-processing unit will greatly reduce the cost and increase the reliability of ion-thruster subsystems, thereby making them more competitive with chemical subsystems. Many of the concepts and results reported here are applicable to ion-thruster subsystems comprised of larger diameter mercury or inert-gas thrusters.

REFERENCES

1. F.J. Wessel and W.S. Williamson, "8-cm Ion Thruster Characterization," NASA CR-167887, January 1983.

2. M.A. Mantenieks, "Extended Performance 8-cm Mercury Ion Thruster," AIAA Paper No. 82-1913 New Orleans, Louisiana, November 17-19, 1982.

3. J.L. Power, "Planned Flight Test of a Mercury Ion Auxiliary Propulsion System I - Objectives, System Descriptions, and Mission Operations," AIAA Paper No. 87-647, San Diego, California, April 25-27, 1978.

4. F.J. Wessel, W.S. Williamson, and C.R. Dulgeroff, "Extended-Performance 8-cm Ion Thruster Operation," AIAA Paper No. 82-1955, New Orleans, Louisiana, November 17-19, 1982.

5. V.K. Rawlin, "Extended Operating Range of the 30-cm Ion Thruster with Simplified Power Processor Requirement," AIAA Paper No. 81-0692, Las Vegas, Nevada, April 21-23, 1981.

6. V.K. Rawlin, "Reduced Power Processor Requirements for the 30-cm Diameter Hg Ion Thruster," AIAA Paper No. 79-2081, Princeton, New Jersey, October 30-November 1, 1979.

7. R.P. Gruber, "Simplified Power Supplies for Ion Thrusters," AIAA Paper No. 81-0693, Las Vegas, Nevada, April 21-23, 1981.

8. F.J. Wessel and D.J. Hancock, "Simplified Power Processing for Ion Thruster Systems," AIAA Paper No. 83-1394, Seattle, Washington, June 27-29, 1983.

DISTRIBUTION LIST

	Copies
National Aeronautics and Space Administration Washington, DC 20546 Attn:	
RP/Mr. Earl E. VanLaningham, MS B600	1
RP/Mr. Robert A. Wasel, MS B600	1
MT/Mr. Edward J. Brazill, MS B326	1
National Aeronautics and Space Administration Lewis Research Center 21000 Brookpark Road Cleveland, OH 44135 Attn:	
Technology Utilization Office, MS 7-3	1
Report Control Office, MS 60-1	1
Library, MS 60-3	2
Dr. M. Goldstein, Chief Scientist, MS 5-9	1
Mr. Dave Byers, MS 500-219	1
Mr. Frank Berkopec, MS 500-220	1
Mr. Jim Stone, MS 500-219	1
Mr. Vince Rawlin, MS 500-220	1
Mr. Carl Aukerman, MS 500-220	1
Mr. Terry Hardy, MS 500-219	1
Mr. Maris A. Mantenieks	10
National Aeronautics and Space Administration Lyndon B. Johnson Space Center Houston, TX 77058 Attn:	
Mr. Hu Davis	1
Dr. James E. McCoy, Code SN3	1
National Aeronautics and Space Administration Marshall Space Flight Center Huntsville, AL 35812 Attn:	
Mr. Robert Bechtel	1
COMSAT Laboratories P.O. Box 115 Clarksburg, MD 20734 Attn:	
Mr. B. Free	1
Comsat Corporation 950 L'Enfant Plaza, S.W. Washington, DC 20024 Attn:	
Mr. Sidney O. Metzger	1

Intelsat
490 L'Enfant Plaza, S.W.
Washington, DC 20024
Attn:
Mr. Rolland Schreib 1

Rocket Propulsion Laboratory
Edwards AFB, CA 93523
Attn:
LKDH/Lt. Phil Roberts, MS 24 1

DFVLR - Institute fur Plasmadynamik
Technische Universitat Stuttgart
7 Stuttgart-Vaihingen
Allmandstr 124
West Germany
Attn:
Dr. Gerhard Krulle 1

Giessen University
1st Institute of Physics
Giessen, West Germany
Attn:
Professor H.W. Loeb 1

Jet Propulsion Laboratory
4800 Oak Grove Laboratory
Pasadena, CA 91102
Attn:
Technical Library 1
Mr. James Graf 1
Dr. Dennis Fitzgerald 1
Dr. John Brophy 1

Electro-Optical Systems, Inc.
300 North Halstead
Pasadena, CA 91107
Attn:
Mr. E. James 1
Mr. W. Ramsey 1

Research and Technology Division
Wright-Patterson AFB, OH 45433
Attn:
(ADTN) NASA Rep. 1

NASA Scientific and Technical
Information Facility
P.O. Box 8757
Baltimore, MD 21240
Attn:
Accessioning Dept. 1

Dept. of the Navy
Office of Naval Research
University of New Mexico
Bandolier Hall West
Albuquerque, NM 87131
Attn:
G. Max Irving 1

Air Force Office of Scientific Research
Bolling AFB
Washington, DC 20332
Attn:
Dr. M. Micci 1

Case Western Reserve University
10900 Euclid Avenue
Cleveland, OH 44106

DST 1
Ministry of Defence
Metropole Building
Nothumberland Avenue
London, WC2 N5BL ENGLAND
Attn:
Dr. D.G. Fearn 1

United Kingdom Atomic Energy Authority
Culham Laboratory
Abingdon, Oxfordshire OX143DB
ENGLAND
Attn:
Dr. P.J. Harbour 1
Dr. A.R. Martin (Rm F4/135) 1

National Aeronautics and Space Administration
Goddard Space Flight Center
Greenbelt, MD 20771
Attn:
Dr. David H. Suddeth 1

Sandia Laboratories
P.O. Box 5800
Albuquerque, NM 87185
Attn:
Mr. Ralph R. Peters, Mail Code 4537 1
Mr. Dean Rovang, Mail Code 1251 1

Ion Tech Inc.
2330 E. Prospect Road
Fort Collins, CO 80525
Attn:
Dr. Gerald C. Isaacson 1
Dr. Dan Siegfried 1

EG & G Idaho
P.O. Box 1625
Idaho Falls, ID 83401
Attn:
Dr. G.R. Longhurst, TSA-104 1

Michigan State University
East Lansing, MI 48824
Attn:
Dr. J. Asmussen 1
Dr. M.C. Hawley 1

The Takagi Research Laboratory
Department of Electronics
Kyoto University
Yoshidahonmachi Sakyo-ku Kyoto 606
JAPAN
Attn:
Dr. Toshinori Takagi 1

Department of Aeronautics
Faculty of Engineering
University of Tokyo
7-3-1, Hongo Bunkyo-ku
Tokyo, JAPAN
Attn:
Prof. Itsuro Kimura 1

Mr. Susumu Masaki
Department of Electronics
Tokyo National Technical College
No. 1220-2
Kunugida-cha, Hachioji 193
Tokyo, JAPAN 1

TRW Inc.
TRW Systems
One Space Park
Redondo Beach, CA 90278
Attn:
Mr. Sid Zafran 1

National Aeronautics and Space Administration
Ames Research Center
Moffett Field, CA 94035
Attn:
Technical Library 1

National Aeronautics and Space Administration
Langley Research Center
Langley Field Station
Hampton, VA 23365
Attn:
Technical Library 1

Princeton University
Princeton, NJ 08540
Attn:
De. Arnold Kelly 1

Boeing Aerospace Co.
P.O. Box 3999
Seattle, WA 98124
Attn:
Mr. Donald Grim, MS 8K31 1

Lockheed Missiles and Space Co.
Sunnyvale, CA 94088
Attn:
Dr. William L. Owens
Dept. 57-24 1

Electrotechnical Laboratory
1-1-4, Umezono, Sakura-Mura,
Niihari-Gun
Ibaraki, JAPAN
Attn:
Dr. Katsuya Nakayama 1

Dr. Pradosh Ray
Tuskegee Institute
School of Engineering
Tuskegee Institute, AL 36088 1

Dr. M. Krishnan
Dept. of Applied Physics
P.O. Box 2159
Yale Station
New Haven, CT 06520 1

Mr. Lee W. Parker
252 Lexington Road
Concord, MA 01741 1

Dr. Chris Olson
Dept. of Physics
University of Huntsville
Huntsville, AL 35899 1

Dr. Kevin Rudolph
MS M0482
Martin Marietta Aerospace
P.O. Box 179
Denver, CO 80201 1

Dr. Ira Katz
Systems, Science and Software
P.O. Box 1620
LaJolla, CA 92038 1

Dr. David Finkelstein
Physics Department
Georgia Institute of Technology
Atlanta, GA 30332 1

Dr. Rod Burton
G-T Devices, Inc.
5705 A General Washington Drive
Alexandria, VA 22312 1

Instiuto de Pesquisas Espaciais - INPE
Library and Documentation Division
C.P. 515
Sao Jose dos Campos - SP
12200 - BRAZIL 1

Mr. Chuck Crawford
Kimball Physics Inc.
Kimball Hill Road
Wilton, NH 03086 1